ANALYSIS OF MIXING DURING HYDROGEN STORAGE IN GAS RESERVOIRS

A RESERVOIR SIMULATION STUDY

by

Robin Johannes Terstappen

In partial fulfilment of the degree of

Master of science
in applied earth sciences

at the Delft University of Technology,
to be defended on Monday September 27, 2021 at 15:00

Thesis committee:

Dr. Prof. D.F. Bruhn	TU Delft	chair/first supervisor
Dr. H. Hajibeygi	TU Delft	second supervisor
Ir. W. Eikelenboom	EBN	first supervisor
Ir. T. Huijskes	EBN	second supervisor
Dr. A. Barnhoorn	TU Delft	committee member

This thesis is confidential and cannot be made public until September 30, 2021.

An electronic version of this thesis is available at http://repository.tudelft.nl/.

TU Delft

Preface

Dear reader,

This thesis work concludes the inspiring trajectory of my master studies in geo-energy engineering, during which I have had the pleasure to work with many joyful and ambitious fellow students and academics. The past nine months have been a challenging endeavor, with both exhausting and satisfying aspects. Before moving on to the actual content of the report, I would like to express my gratitude to all that have supported me during the process.

First, I wish to thank my EBN supervisors Ir. Walter Eikelenboom, and Ir. Thijs Huijskes, with whom I have had countless supportive meetings, conceptualizing the theory, methods and goals. Throughout the meetings, which have at times been on a daily basis, the two of you have supported me in a constructive yet critical way, bringing positivity to the project whenever needed. The cooperation between EBN and TUDelft has resulted in various exciting discussions during the progress meetings, with participating members from both parties. The interests of the company and the university were well aligned, and never negatively interfered with the project. I would like to thank Prof. dr. David Bruhn for his empathy, and understanding my doubts. Your vast experience in supervising master students was reflected in our meetings, during which you helped me to structure the writing of the report, and focus on the bigger picture. These meetings often provided me with new energy. I would also like to thank Prof. Hadi Hajibeygi for his constructive feedback and scientific input in the project. You managed to assemble an inspiring team of young academics in the Admire group. Participation in their monthly meetings has given me the opportunity to share issues with people working on related subjects, for which I am grateful.

Furthermore, I would like to thank my family, friends, and girlfriend in particular, for their unconditional support, patience, and refreshing moments.

R.J.Terstappen
's-Gravenhage, September 2021

Abstract

This thesis contributes to increasing the technology readiness level of hydrogen storage in gas reservoirs, which will be required when hydrogen has become a major energy carrier in the future Dutch energy system. It addresses the mixing processes with resident gases that occur during hydrogen storage operations in gas fields, and analyzes their implementation in a reservoir simulator. The CMG GEM reservoir simulator allows incorporation of mechanical dispersion and effective molecular diffusion into its simulations, while solving the advection dispersion transport equation fully implicitly, as well as gravitational segregation and other macro scale mixing phenomena. Mechanical dispersion is quantified by its main parameter dispersivity, for which a large uncertainty exists in the literature. Dispersivity represents pore scale fluid velocity differences caused by microscale heterogeneities in a porous medium. Due to the lack of adequate hydrogen dispersivity experiments, a range of dispersivity values is collected from literature on (groundwater) dispersivity experiments in sandstones. A sensitivity analysis is conducted, in which the influence of the different mixing processes on the mixing between working gas and cushion gas is analyzed. For this, a conceptual reservoir model (radial and homogeneous), with properties based on Dutch sandstone gas fields was built in CMG GEM. The effect of molecular diffusion on mixing proves to be negligible compared to mechanical dispersion at typical reservoir flow rates. Furthermore, the results of the simulations prove to be significantly influenced by numerical dispersion, which is a calculation error, dependent on grid size and time step. The effect of numerical dispersion compared to mechanical dispersion is quantitatively analyzed, after which various options are introduced to deal with numerical dispersion in a way that the physical processes are most realistically represented. The work in this thesis demonstrates the challenges of realistically implementing hydrogen storage mixing processes in a reservoir simulator, and should be regarded as a foundation for further research.

Contents

List of Figures

‘

List of Tables

List of Abbreviations

α_m	isentropic dispersivity of phase m
λ	mobility
μ	viscosity
Ω	temperature dependent collision integral
Φ	flow potential
ϕ	porosity
ρ_m	molar density of phase m
σ_{12}	average collision integral
$\vec{v}_m$	flow velocity of phase m
B	formation volume factor
C_{im}	concentration of component i in phase m
d	depth
D_0	diffusion coefficient in air
D_e	effective molecular diffusion
D_h	hydraulic (physical) dispersion
D_{iq}	dispersion coefficient of component i
D_m	mechanical dispersion
$erfc$	complementary error function
g	earth gravitational constant
k_h	horizontal permeability
k_v	vertical permeability
L	reservoir length
m	cementation factor
n	distance between two grid points
N_{pe}	peclet numer
Nm^3	cubic meter at standard conditions
p	pressure
P_{cwg}	gas-water capillary pressure
Q	mass flow rate
r	reservoir radius
S_m	saturation of phase m
t_D	dimensionless time
T_i	transmissibility of phase i
u	flow velocity
y_{ij}	mole fraction of component i in phase j
A	empirical coefficient equal to 1.859
M	molar mass

1 | Introduction

1.1. Hydrogen in the future Dutch energy system

Current global energy systems have led to climate change and environmental problems [6]. These issues demand a switch from the currently exploited hydrocarbon energy sources to new sustainable ones. During the Paris climate agreement in 2015, the UN has defined net zero greenhouse gas emissions as the global goal for 2050, and a reduction of 49% by 2030 compared to the levels of 1990 [6]. During the year 2021, the European Union has even updated their CO_2 emission reduction target to 55% in 2030 compared to the 1990 level [7]. Therefore, the greenhouse gases, which are emitted with the use of conventional energy resources have to be reduced, and the need for sustainable energy is increasing. However, some of these sustainable energy resources, such as wind solar, are intermittent by nature [8]. Due to unsynchronized fluctuations on the demand and supply side, there exists an overproduction (and underproduction) of energy at times, which cannot be fully utilized unless large scale storage technologies are developed. It is of societal and economical relevance to find an adequate energy storage medium, in order to create a balanced energy system.

Even in a successful future energy market, where a significant part of the energy demand is produced by renewable energy sources (RES), the energy mix will need to consist of a relatively large part of liquid and gaseous energy carriers for transport and storage of energy [8]. A schematic overview of an example future energy system in the Netherlands is given in fig. 1.1. The mentioned gaseous and liquid forms will be needed in industries where electricity and battery-based energy supply alone is insufficient [8], and energy is needed in molecular form. Examples are fuel for the aviation and shipping industry, and high temperature heat for industrial processes. There will also be a demand for hydrogen in the process industry, for the synthesis of chemical products and materials. The current contribution of molecular energy carriers to the Dutch energy supply is around 80 percent [8], which is formed for a large part by natural gas. The contribution of molecular energy is expected to reduce to 40-60 percent in 2050, which is expected to include a high contribution of hydrogen gas [8]. Hydrogen gas can be produced from electricity through electrolysis, or from methane by steam methane reforming [8], as displayed in fig. 1.1. Consequently the hydrogen needs to be stored in adequate volumes until demanded further applications. The stored hydrogen could be used directly as a replacement for natural gas, if used for domestic heating or to produce electricity in gas-driven power plants. The hydrogen gas can also be used combined with sustainable forms of carbon, in order to produce synthetic liquid fuels and chemicals. In combination with nitrogen and carbon, a huge variety of chemical products and materials can be created [8].

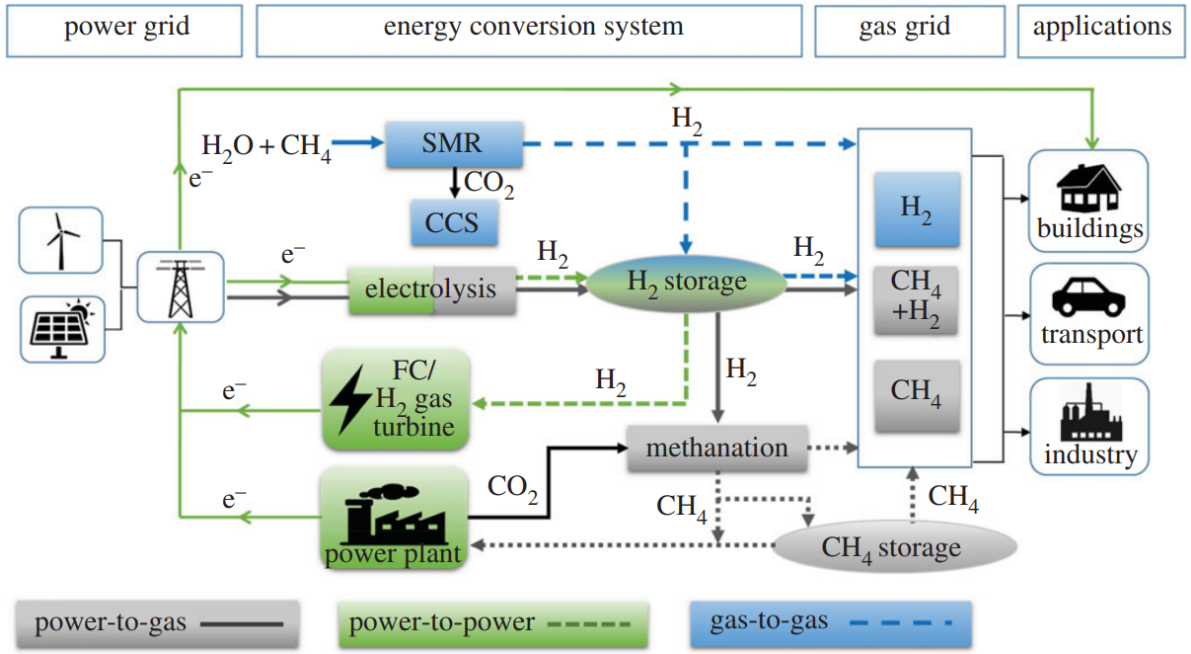

Figure 1.1: Schematic overview of the main energy pathways in a possible future energy system, in which hydrogen plays a role as energy carrier. [1]

1.2. SUBSURFACE STORAGE POTENTIAL FOR HYDROGEN IN THE NETHERLANDS

If hydrogen is to fulfill its role of energy carrier in the future energy system, storage of large quantities of hydrogen gas needs to be enabled. The most obvious solution might seem to store hydrogen in industrial tanks. However, the expected demand for storage capacity substantially exceeds the volume of such tanks. This is where subsurface formations could come in as part of the solution [5]. The Dutch onshore and offshore subsurface has been heavily exploited primarily for its gas resources throughout the past decades [9]. The remaining gas reservoirs have proven to be effective in storing billions of cubic meters of natural gas for millions of years without complications. [9]. Therefore they have the potential to be used as a large scale Underground Hydrogen Storage (UHS). However, because of the different physical and chemical properties of hydrogen gas compared to natural gas, a lot of research and experimenting has to be conducted before the Technology Readiness Level (TRL) is elevated enough for hydrogen storage in gas reservoirs to be realized. Another hydrogen storage option is provided by salt caverns, which have proven their functionality during UHS operations in the USA and UK [10]. However, the availability of (enough) developed salt caverns poses a challenge, which is further elaborated in the paragraph below.

TNO and EBN, which are Dutch organizations working on subsurface energy subjects, have performed a study regarding the underground energy storage potential in the Netherlands [11]. One of their findings is that a total working volume of 93 billion Nm^3 in onshore, and 60 billion Nm^3 in offshore gas fields is potentially available for cyclic hydrogen gas storage [11]. An additional 14.5 billion Nm^3 of hydrogen gas working volume could be available in 321 onshore underground salt caverns [11]. However, the availability of these caverns for hydrogen storage is for a large part restricted by their development rate [11]. Estimates from their latest report indicate that up to 65 salt caverns could technically be developed for hydrogen storage by 2050 [2]. However, the development of this number of salt caverns in a relatively short time span will most likely be opposed by significant political and social resistance. For the reasons mentioned, a maximum working gas volume (part of the storage gas that can be recovered) of roughly 5 billion Nm^3 could be realised by 2050 in Dutch salt caverns. The study by TNO and EBN predicts the demand for hydrogen gas storage in 2050 to be between 1 and 10 billion Nm^3, based on energy balancing for a normal weather year, without strategic reserves for security of supply [2]. This means that even if salt caverns would be the subsurface structures of preference for hydrogen storage, given their proven functionality in salt domes in the USA and the UK [10], chances are still significant that additional storage capacity is needed, which could potentially be provided by gas reservoirs. The division of hydrogen storage between salt caverns and gas reservoirs is displayed in fig. 1.2. This diagram displays four possible energy system development pathways from 2020 to 2050, in

which hydrogen plays an increasingly significant role as energy carrier moving from pathway A to D. Where the utilization of gas reservoirs as storage media is optional in pathway B, it is a necessity in pathways C and D due to the limited capacity of salt cavern development.

Taking section 1.1 and section 1.2 into account, it becomes clear that research regarding underground hydrogen storage (UHS) in gas reservoirs has a significant societal relevance in the Netherlands. Hydrogen may play an important role in the future Dutch energy system, because it can function as energy carrier in an energy system where intermittent sources are dominant. In order to store the demanded volume of hydrogen for the future Dutch energy system, the storage volume that gas reservoirs can provide might be essential.

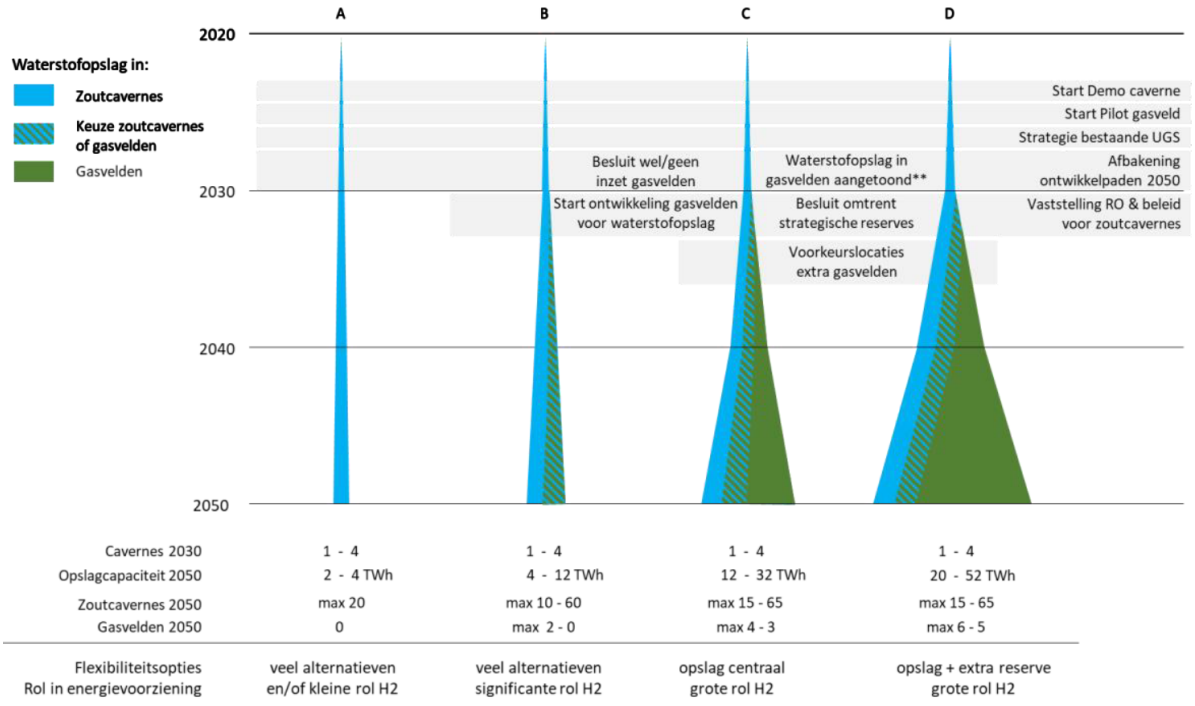

Figure 1.2: Diagram of four 2020-2050 development pathways and corresponding hydrogen storage capacity, divided over salt caverns and gas reservoirs. The presumed hydrogen storage capacities of salt caverns and natural gas reservoirs for this study are 250 GWh and 8 TWh respectively [2].

1.2.1. CHALLENGES FOR UNDERGROUND HYDROGEN STORAGE

The possible future storage of hydrogen in gas reservoirs however, comes with a number of societal and technological challenges, the most important of which are: [12] [13]

- Cap rock integrity
- Well integrity
- Biochemical activity
- Mixing behavior
- Legislation
- Economics

Cap rocks, which form the seals of subsurface reservoirs, have prevented the escape of natural gas from reservoirs for millions of years [14]. In the case of storing hydrogen in these reservoirs, new challenges arise. Hydrogen has been found in several gas reservoirs, proving that certain reservoir types are capable of constraining hydrogen molecules for a long time period [13]. However, due to its smaller molecules [13], hydrogen has a higher potential to leak though faults and cap rocks and wells than the natural gas. Another risk of losing hydrogen is formed by diffusion through formation water in the reservoir. Hydrogen has a high potential for

diffusion because of its high diffusivity [13].

Concerning the challenge of the biochemical activity of hydrogen; the temperature and pH conditions in a gas reservoir are usually not sufficient for hydrogen to cause a significant chemical reaction in combination with molecules of the reservoir rock [12]. However, hydrogen is a universal electron donor for the metabolism of different anaerobic microbial species. Therefore, the presence of hydrogen in combination with subsurface reactants like sulfides, sulfates, carbonates and oxides, causes hydrogenothrophic microbial processes to take place. These processes could cause irreversible losses of hydrogen, and create components like CH_4, CH_3COOH and H_2S [12].

The challenge around legislation of UHS is one that will require awareness in times to come. The hydrogen supply chain is expected to develop into a network similar to the natural gas network. The Dutch government will review whether, and under what conditions, part of the natural gas network could be re-used for hydrogen [5]. This will most likely be done in cooperation with the network operator. Furthermore, it is not yet clear if the demanded storage capacity for hydrogen in gas reservoirs will be permitted by the Dutch government.

The economical investment in cushion gas for hydrogen storage has to be taken into account in the financial plan of a hydrogen storage project. Depending on the volume ratio between cushion gas and working gas (hydrogen) in a UHS facility, and the type of cushion gas and its volumetric value at a specific moment in the future, certain projects could be to a greater or lesser extend economically feasible [10]. Moreover, a comprehensive natural gas infrastructure has been developed in Europe over the past decades, consisting of pipelines and underground production and storage facilities[15]. It has yet to be proven whether the same network could partly be transformed into a hydrogen network in an economically feasible way. Another economic aspect to consider, is that if a very large hydrogen storage capacity is to be fulfilled, it might not be possible to develop the full capacity in the more easily accessible shallower gas fields, which have a relatively high porosity. Instead, some of the deeper fields might need to be utilized, requiring more complicated and expensive wells, and powerful more expensive compressor pumps [15].

Although the other mentioned challenges around UHS operations are recognized, this thesis focuses on the processes leading to mixing of hydrogen and a cushion gas, and the differences between a simulated model and the reality. Cushion gas is defined as the volume of gas which is not produced and therefore remaining in the storage medium. It undergoes alternate compression and expansion during the injection and withdrawal cycles respectively, accomodating the required pressure and production rate of the stored gas [10]. The mixing behavior of hydrogen and a cushion gas is of importance because mixing of their molecules, which is inevitable during miscible displacement, leads to an irreversible loss of hydrogen. The process of mixing between cushion gas and working gas molecules, during which a mixing zone develops, is illustrated in fig. 1.3. It is important that the purity of the produced hydrogen is maintained, in order for it to be used in most further applications, such as for fuel cells or the chemical industry [8]. So it is of critical importance to understand the processes of mixing and their adoption in a reservoir simulator, in order to make realistic predictions.

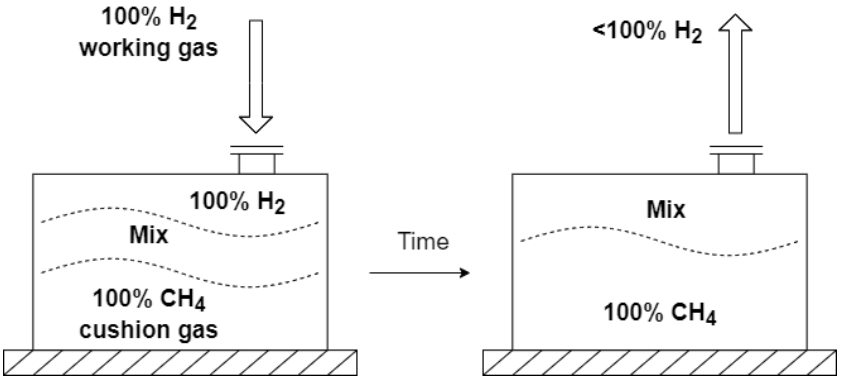

Figure 1.3: Conceptual visualization of a hydrogen storage cycle. Mixing zone develops at mixing front between injected hydrogen and the cushion gas, causing the mole fraction of the recovered hydrogen to become less than 100% at some point during the production.

1.3. SCIENTIFIC RELEVANCE OF THIS RESEARCH

The societal relevance of increasing the Technology Readiness Level on hydrogen storage in gas reservoirs is discussed in section 1.1, as well as the associated societal and technological challenges. An extensive literature review is conducted in order to identify possible knowledge gaps regarding the processes leading to mixing of hydrogen and a cushion gas. Subsequently, a table is constructed to assemble the most important literature with their specific subjects and main findings. This table is included in the appendix of this report as fig. C.1 and fig. C.2.

The studied literature and their most important findings are summarized in fig. C.1 in the appendix. Out of the 25 publications listed in fig. C.1, 14 are at least partly focused on the process of mixing of hydrogen or natural gas with either residual reservoir fluids or intentionally injected cushion gas. Out of these 14 papers, Hagemann *et al.* 2015 [16], Pfeiffer and Bauer 2015 [17], Feldmann *et al.* 2016 [18] and Sainz-Garcia *et al.* 2017 [19] have focused on UHS in aquifers. Only Feldmann *et al.* 2016 [18] and Hagemann 2018 [20] have focussed (partly) on mixing processes during UHS in gas reservoirs.

Both aquifers and gas reservoirs have the potential to be developed into an UHS. However, the development of an UHS in aquifers would differ from those in gas reservoirs [20]. For UHS in aquifers a gas volume has to be formed during development, for which the aquifer water should be displaced by the injected gas. The efficiency of the displacement between two immiscible fluids depends mainly on the differences in density, viscosity and surface tension forces [20]. The two fluids will form a two phase flow system, which has very different displacement characteristics compared to the miscible single phase flow system of gas reservoirs [20]. In gas reservoirs, part of the natural gas will have remained in the reservoir. If the inflow of aquifer brine into the reservoir at the time of production was weak, the residual gas saturation could be nearly as high as the initial gas saturation, although the pressure would have decreased during depletion [20]. In that case the residual natural gas will have to be displaced by the injected cushion gas or hydrogen.

This thesis will focus on UHS in gas reservoirs instead of aquifers. Therefore, the system will contain a single phase flow with miscible gases of two components. However, the process of gravitational segregation, which is discussed in the literature on UHS in aquifers, is also applicable to UHS in gas reservoirs. This makes the literature on UHS in aquifers, which is more abundant, valuable for this thesis. Hagemann 2018 [20] concludes that gravitational segregation can complicate the efficient displacement of the native fluid during UHS in both aquifers and gas reservoirs, although the effect is significantly stronger in aquifers due to the larger density difference between hydrogen and water than between hydrogen and residual natural gas. Viscous fingering however, is a process that only occurs in multi phase flow systems, and therefore only complicates the native fluid displacement during UHS in aquifers, and not in gas reservoirs.

The studies of Srinivasan 2006 [21] and Blicharski and Rybicki 2008 [22] have focussed on mixing processes in underground natural gas storage systems (UGS), where experiments have been conducted with tracer injections and reservoir simulations. In the tracer experiments the concentration of a tracer molecule injected at one location in the reservoir is measured during production from another location [22]. Blicharski and Rybicki 2008 [22] have determined values for the effective molecular diffusion and dispersivity by comparing calculated and measured concentrations. The concentrations were calculated by a solution to the radial convection-dispersion equation. The convection-dispersion equation is not specific for natural gas but is used to describe fluid movement in all gas-gas interactions [23]. Therefore, the literature on mixing processes during UGS operations is relevant for UHS operations too.

Mechanical dispersion can be quantified by the dispersivity parameter, which is mentioned in Feldmann *et al.* 2016 [18]. These authors mention mechanical dispersion, amongst mobility ratio's, density differences, and effective molecular diffusion, as the most important phenomena leading to mixing during UHS operations. The mobility ratio is said to be of lesser influence during gas-gas mixing than during mixing in aquifers. This is because the miscibility leads to a high dispersion of the mixing front, which acts as stabilizing force [18]. Effective molecular diffusion is considered as a slow process when compared to advective/convective transport [18]. Therefore, the density difference and mechanical dispersion are considered to be the two most important mixing processes during UHS in gas reservoirs. The authors mention that the mechanical dispersion is mainly determined by the dispersivity parameter, which is a measure of the heterogeneities ranging from pore to field scale. According to Gelhar *et al.* 1992 [4], dispersivity is strongly dependent on the considered

length scale, and therefore labarotory measurements cannot directly be transferred to the reservoir scale. According to Feldmann *et al.* 2016 [18], the dispersivity ranges from 1m to 100 m. However, after mentioning the importance of this parameter in the theoretical concepts, the influence of the dispersivity on the extent of mixing in UHS is not further discussed in their writing or that of any others, creating a knowledge gap.

The effect of the density difference between hydrogen and formation water on the extent of mixing has been analyzed by Sainz-Garcia *et al.* 2017 [19], Hagemann *et al.* 2015 [16], and Hagemann 2018 [20], where gravitational segregation was shown to be an influential process. The effect of density difference between hydrogen and a potential cushion gas in UHS in gas reservoirs has only been analyzed by Feldmann *et al.* 2016 [18], where they focused on the displacement of hydrogen through a heterogeneous reservoir in multiple storage cycles. However, the effect of operating pressure, permeability, and reservoir dimensions on the gravitational segregation process hasn't yet been analyzed, forming another knowledge gap.

Furthermore, the numerical modeling of the mixing interaction between gases in UHS operations involves numerical dispersion. Numerical dispersion is a truncation error of the simulator which intrinsically causes smearing out of the molecular composition over grid cells. This causes mixing to appear more significant in the simulator than it is in reality [23]. Fanchi 1983 [24], amongst others, has done research on this topic with respect to miscible and immiscible displacement in enhanced oil and gas recovery [23]. A literature gap is formed by the subject of numerical dispersion related to UHS operations in gas reservoirs. The effects of numerical dispersion on hydrogen storage simulations have not yet been analyzed.

From the literature discussed above, three mixing processes occurring in underground hydrogen storage in gas reservoirs are distinguished, which are:

- Gravitational segregation (mixing at macro/reservoir scale)
- Mechanical dispersion (mixing at micro/molecular scale)
- Effective molecular diffusion (mixing at micro/molecular scale)

With this thesis I wish to contribute to filling the mentioned literature knowledge gaps concerning the mixing processes related to UHS in gas reservoirs, which are repeated below:

- The range of the physical dispersion (mechanical dispersion and effective molecular diffusion) between two gases in an UHS, and its effect on the mixing.
- The effect of operating pressure, permeability, and reservoir dimensions on the gravitational segregation process.
- The effects of numerical dispersion in UHS simulations.

1.3.1. OBJECTIVE AND MAIN RESEARCH QUESTION

The objective of this thesis is to contribute to filling the knowledge gaps mentioned above, in order to gain insight in underground hydrogen storage in gas reservoirs. This may contribute to increasing the Technology Readiness Level (TLR), which is required before a project pilot may be realized [11]. As mentioned earlier in section 1.2.1, a critical aspect in UHS in gas reservoirs is the purity of the recovered hydrogen. Early breakthrough of cushion gas will result in the recovery of impure hydrogen at the production well. Therefore, this study will mainly focus on the mixing behavior of hydrogen with a cushion gas. The main research question supporting this topic is:

- How can the mixing processes related to underground hydrogen storage in gas reservoirs be simulated in a realistic way?

1.3.2. RESEARCH APPROACH

The main research question mentioned in section 1.3.1 needs a solid research approach in order for it to be answered in this thesis. The first step is to conceptually study the functioning of the mixing processes mentioned in section 1.3. Subsequently, a way to realistically capture these mixing processes in a reservoir simulator should be determined. These steps produce the following three sub research questions:

- What is the significance of gravitational segregation for UHS in gas reservoirs, and how can this mixing process realistically be captured in a reservoir simulator?
- What is the significance of mechanical dispersion for UHS in gas reservoirs, and how can this mixing process realistically be captured in a reservoir simulator?
- What is the significance of effective molecular diffusion for UHS in gas reservoirs, and how can this mixing process realistically be captured in a reservoir simulator?

The implementation of physical mixing processes in a reservoir simulator implicates numerical dispersion [23]. The role of numerical dispersion relative to physical dispersion, the latter of which consists of mechanical dispersion and effective molecular diffusion, should be quantified in order for it to realistically be included in the calculation. This produces the following additional sub research questions:

- How does numerical dispersion quantitatively relate to physical dispersion?
- How can physical dispersion realistically be simulated, taking into account the effects of numerical dispersion?

By following this research approach, substantial steps should be made towards the research goal and answering the main research question.

1.4. REPORT OUTLINE

In this section, the structure of the report, as displayed in fig. 1.4 is discussed in order to create clarity for the reader. After the introduction, the report starts with an extensive elaboration on the the relevant theoretical concepts. The theoretical concepts section contains a small number of illustrative experiments and results, in order to clarify some of the used concepts and equations.

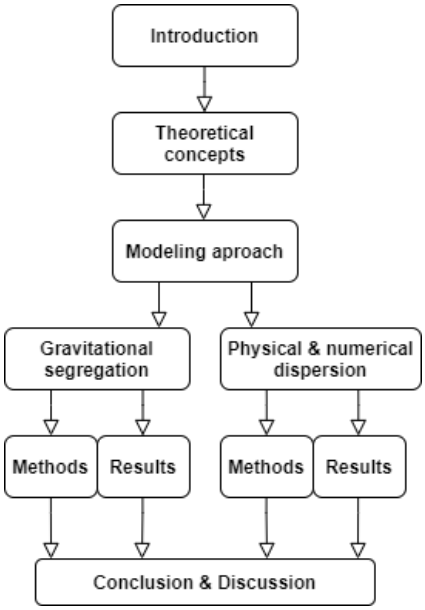

Figure 1.4: Flow diagram of the report chapters

The theoretical concepts chapter is followed by a modelling approach chapter, in which a base case reservoir model is introduced with its accompanying parameters and settings. This base case model is referred to and used in later chapters, with the advantage that only mutations have to be mentioned if most characteristics are identical. Furthermore, the modelling approach chapter discusses the software that is used to model the mixing behavior during UHS, including its material balance transport equation and a workflow diagram and description.

Subsequently a separate chapter is included on the modelling experiments on each of the mixing processes that were introduced in the literature review of section 1.3, where effective molecular diffusion and mechanical dispersion are combined as one. Each of these chapters consists of its own methodology and results section with a number of simulations/experiments. The methodology sections of these chapters specify the earlier modeling approach chapter.

The report is completed by a conclusion, discussion and recommendations chapter, regarding the topics from both previous chapters.

2 | Theoretical concepts

2.1. Introduction to UHS mixing processes

When storing hydrogen in gas reservoirs, the operating pressure of the field must remain at a sufficient level to meet a certain demanded production rate. This operating pressure can be provided by a cushion gas, which will remain in the reservoir. During UHS operations, using the same cushion gas and working gas (hydrogen) is practically unfeasible due to the high production costs of hydrogen and the inability to recover 100% of the present natural gas from a reservoir [25]. Therefore, mixing of cushion gas molecules with hydrogen (working gas) molecules is an important aspect of hydrogen gas storage, which influences the recoverable fraction of injected hydrogen, as shown in fig. 1.3 . The cushion gases considered in this thesis are CH_4, CO_2, and N_2, because of their natural occurrence in gas reservoirs, high density, and low cost, respectively [26].

When one miscible fluid is displacing another, mixing will take place. After an initial sharp interface between the two fluids, a so called mixing zone develops at the mixing front where the two fluids make contact [27]. The mixing zone will grow as the displacement continues, and the differences in physical properties will balance out in time. The rate at which the mixing zone grows and at which the front propagates is dependent on advective and diffusive forces. Advection determines how fast a tracer travels together with the pressure driven fluid flow. Dispersive and diffusive processes are driven by concentration gradients and / or the spatial variation of flow velocities that determine the proportion of spreading [27]. The type of mixing front during liquid-gas or liquid-liquid interaction is dependent on the mobility ratio, which is defined as the viscosity of the displaced fluid divided by the viscosity of the displacing fluid. An unfavorable ratio can result in viscous fingering. However, in this thesis only relatively low liquid saturated gas reservoirs are considered, preventing fingering in the fluid interaction.

2.2. Advection-dispersion equation

As mixing of the gases is caused by advective-diffusive forces, this is an important subject to analyze. The following advection-dispersion equation 2.2.1 captures the described mixing processes.
[3]

$$\phi \frac{\partial C}{\partial t} + \nabla C u - \nabla (D_h \nabla C)\phi = 0 \tag{2.2.1}$$

2.3. Hydraulic/physical dispersion

In eq. (2.2.1), $\nabla C u$ describes advective process, and $\nabla(D_h \nabla C)\phi = 0$ describes the dispersive and diffusive processes. D_h is the hydrodynamic (physical) dispersion, which is defined below as the sum of effective molecular diffusion and mechanical dispersion [27] in eq. (2.3.1).

$$D_h = D_m + D_e = \alpha * u + D_0 \phi^m \tag{2.3.1}$$

The two components forming the total hydrodynamic dispersion (also called physical dispersion) (D_h) described by eq. (2.3.1), are effective molecular diffusion (D_e) and mechanical dispersion (D_m). D_m only exists if pressure driven fluid flow takes place. Tortuosity and varying diameters of pore channels make flow spread out and travel faster in some pores than others, causing transversal and longitudinal mechanical dispersion, as explained in fig. 2.1.

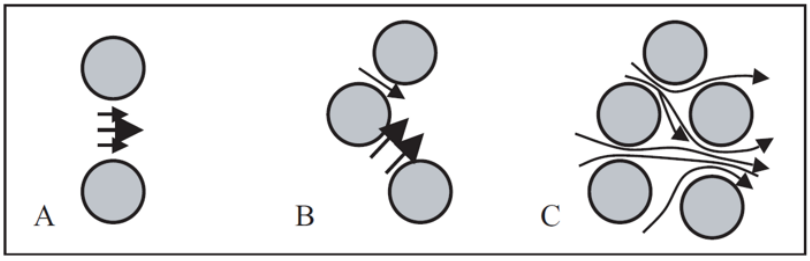

Figure 2.1: Conceptual visualization of mechanical dispersion. A: velocity variations within single pore due to wall-effects, B:pore size distributions, C:turtuosity effects. [3]

Transverse dispersion also occurs in porous media and is described by a transverse dispersion coefficient; however, under most conditions transverse dispersion is observed to be much less significant than longitudinal dispersion and is not considered further here [3]. Therefore, in the rest of this report, the longitudinal variant is meant whenever dispersion or dispersivity is mentioned. Dispersion is independent on the solute and highly dependent on the porous medium and its heterogeneity. Effective molecular diffusion is mixing caused by isotropic Brownian motion of fluid and will occur even in the absence of flow between two miscible fluids. Brownian motion can be explained as following: if volume A of two adjacent, equally sized volumes A and B contains twice as many particles as B, at that instant the probability of particles leaving A to enter B is twice that of particles leaving B to enter A. The tendency to move is caused by random oscillations, and over time the concentration is balanced out within the total volume of two miscible fluids [28]. Diffusion will take place with lower speed in a porous medium than in an open volume. The reduction of the effective molecular diffusion (D_e) relative to the diffusion coefficient in air (D_0) is due to the presence of the solid-phase media, resulting in smaller cross-sectional area available for diffusion, the tortuosity of the gas pathways, the presence of disconnected pores, and, at least in dry porous media, the geometry of the pores, as influenced by particle shape [3]. The diffusion decreases with increasing pressure and increases with increasing temperature due to lower and higher molecule movement respectively [28].

Here α is the so called dispersivity, which is measured in the unit meters. Dispersivity is a parameter which determines the local variations in velocity of a fluid in a (subsurface) porous medium, having a transversal and a longitudinal component. The dispersivity is a scale dependent parameter, meaning that its value is dependent on the (cell) scale it is measured for [29]. The exponent of ϕ^m is the dimensionless cementation factor, which defines the diffusive resistivity caused by the network of pores, and is in practice ranged between 1.3 and 3.0 for most subsurface porous media [27] [30]. Due to the velocity dependence of D_m and velocity independence of D_e, the contribution of diffusion to the hydrodynamic dispersion at high flow velocities is negligible. Inspection of eq. (2.3.1) and eq. (2.5.6) shows that the diffusion contribution to D_h is solute dependent, while that of mechanical mixing is not. Thus, the magnitude of dispersion will vary as a function of the solute when diffusion provides a significant contribution, with lower molecular-weight gases exhibiting greater dispersion. Conversely, dispersion is solute-independent for larger velocities, when mechanical mixing dominates dispersion. [3]

2.4. SCALE DEPENDENCY OF DISPERSIVITY

As mentioned in section 5.1, the dispersive process can be incorporated in the GEM simulator by entering a dispersivity value in meters. It is essential to predictions in miscible fluid movement that the dispersivity at a particular site is characterised [4]. It is concluded from both theoretical and experimental investigations that field-scale dispersivities are several orders of magnitude larger than lab-scale values for the same material [4]. This difference is caused by natural heterogeneities, which produce irregular flow patterns and spreading of the solute at field scale. Dispersivity is a parameter that has been the topic of discussion in the literature (e.g., Arya *et al.* 1989 [31], Gelhar *et al.* 1992 [4], Schulze-Makuch 2005 [29] and Molz 2015 [32]). Gelhar *et al.* 1992 [4] collected experimental field-data on dispersivity from earlier publications by other authors, and reinterpreted the reliability and meaning of these data. The reliability judgement is based on the following experiment characteristics:

1. Flow conditions of tracer test
2. Certainty of tracer concentration

3. Tracer type must be non-reactive, in order not to complicate the governing equations
4. Number of dimensions of the tracer concentration input/measurement
5. Method of analysis of the concentration data

The field-scale dispersivity values were determined from experiments with different types of tracers, which were injected at one location of a reservoir, after which the concentration was measured at another location in the reservoir. Injection and measurement of the concentration could be at a single point location or extended over one or more dimensions, which is related to reliability criterium 4 above. The longitudinal dispersivity dataset collected by Gelhar *et al.* 1992 [4] shows a pattern of increasing dispersivity at increasing experimental scale, which could be due to inclusion of more heterogeneity at larger scales. For all experimental data in Gelhar *et al.* 1992 [4], the type of porous medium is defined. However, no specifications have been written down on the lithological properties, which increases the uncertainty for comparison with gas reservoirs in the Dutch subsurface. All datapoints representing sandstone field experiments are displayed in fig. 2.2 as longitudinal dispersivity versus measured scale.

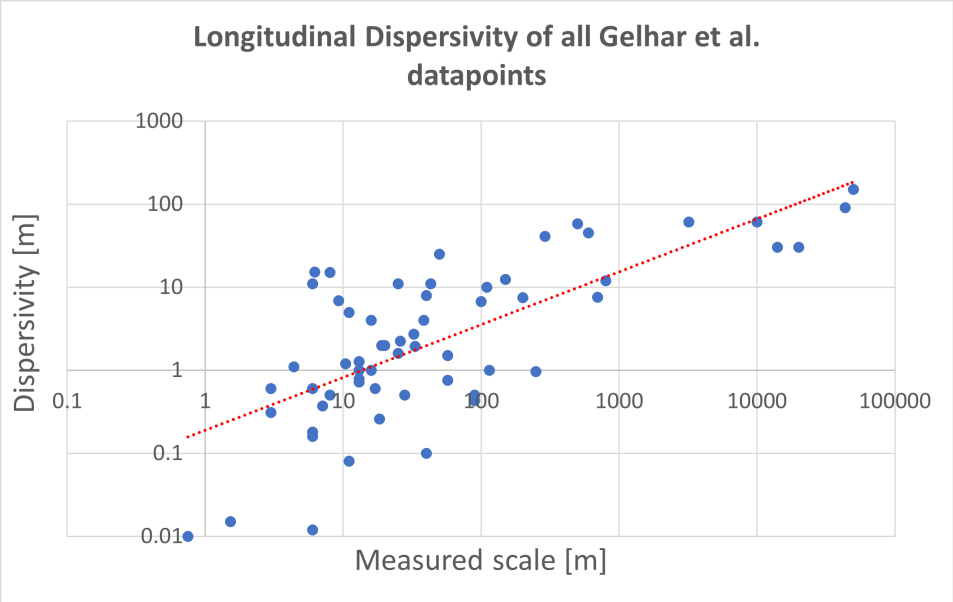

Figure 2.2: All Gelhar et al. longitudinal dispersivity datapoints collected from sandstone fields as function of the scale over which they are measured. The trendline of increasing dispersivity with scale is depicted in red. [4]

However, it is suggested that reliable data should be developed at larger scales in order to establish the nature of the scale dependence [4]. To my knowledge, there exist no reliable dispersivity data beyond a scale of 300 m because no experiments beyond that scale have been conducted with a well defined solute input. Almost exclusively all experiments at that scale have been conducted as either a simulation experiment or analyze the dispersion of natural environmental tracers, meaning that the input is poorly constrained and uncontrolled. When the longitudinal dispersivity data are classified according to the earlier stated reliability judgement, the pattern regarding scale dependency of dispersivity is less clear. All datapoints representing reliable sandstone field experiments are diplayed in fig. 2.3 as longitudinal dispersivity versus measured scale.

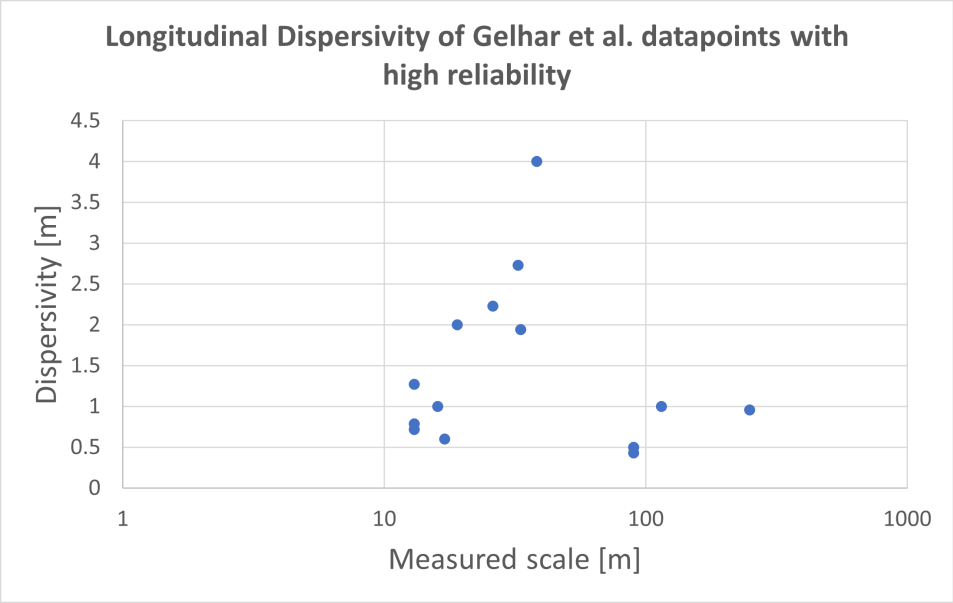

Figure 2.3: Only the most reliable Gelhar et al. longitudinal dispersivity datapoints from sandstone fields. No trendline can be distinguished. Mind the logarithmic scale on the x-axis. [4]

The authors mention that it is not appropriate to represent the longitudinal dispersivity data by a single line because they depend on many field specific factors. Moreover, it is concluded by the authors that the lower range of longitudinal dispersivity values at any scale are more likely to be realistic for field applications [4].

From the abundant literature that was reviewed on the topic of dispersion, it became clear that none of the authors was totally sure of specific dispersivity values being applicable at specific reservoir scales, especially at a scale larger than 300 m. This is due to the fact that many different methods of monitoring, tracer input and data interpretation have been used. Furthermore, there are no reliable data for dispersivity values at a reservoir scale larger than 300 m, which reflects the fact that there are no experiments beyond that scale with a well defined solute input. Most of them are either simulated experiments or field experiments in which an environmental tracer is observed, for which the solute input is ill-defined because it is naturally present in the subsurface instead of being injected.

2.5. 1D ADVECTION & DISPERSION

For an open one-dimensional single phase flow system in which the speed is assumed to be constant due to sufficient reservoir length, the hydrodynamic dispersion D_h is also constant and eq. (2.2.1) is derived to eq. (2.5.1) as shown in appendix A[33].

$$\frac{\partial C}{\partial t} + \frac{u_x \partial C}{\phi \partial x} - (D_m + D_e)\frac{\partial^2 C}{\partial x^2} \tag{2.5.1}$$

The dispersion coefficient D_h for a 1D system is constant because of the assumed homogeneity at the reservoir scale. Nevertheless, at the pore scale heterogeneity exists, which is the cause for dispersion. Another assumption in eq. (2.5.1) is that the retardation factor R_f, through which the diffusion part of the equation should be divided, is equal to 1. Retardation is a phenomenon due to the adsorption of chemical species on the surface of the porous medium. If $R_f > 1$, then the transport of the species is retarded and the effective D_h and U_x are reduced. Furthermore, C is the concentration of the injected fluid, and U_x is the flow speed. eq. (2.5.1) is subject to the following boundary conditions.

$C(x,0) = C_i$ (At initial time, all locations have the initial concentration)

$C(0,t) = C_j$ (At the initial location, the concentration is always that of the injected fluid)

$C(inf, = C_i$ (At infinite distance from the injector, concentration remains the initial concentration)

The dimensionless equation obtained by chain rule multiplication is written below in eq. (2.5.2)[33].

$$0 = \frac{\partial C_D}{\partial t_D} + \frac{\partial C_D}{\partial x_D} - \frac{1}{\frac{u_x L}{\phi D_h}} \left(\frac{\partial^2 C_D}{\partial x_D^2} \right) \tag{2.5.2}$$

$$N_{pe} = \frac{u_x L}{\phi D_h} \tag{2.5.3}$$

The Peclet number, shown in eq. (2.5.3), is defined as the non-dimensional ratio between advective and dispersive forces. The magnitude of the Peclet number is inversely proportional to the degree of dispersion. Thus, low Peclet numbers correspond to a large degree of solute spreading. As explained in section 2.2, at high flow velocities, the contribution of the diffusion to the hydrodynamic dispersion is negligible. Therefore, at high flow velocities, the Peclet number becomes independent on velocity variations. In that case, the Peclet number depends solely on the properties of the porous medium, as represented by the dispersivity (α), porosity (ϕ) and the characteristic length of the system (L). The dimensionless parameters in eq. (2.5.2) are defined as in appendix A.1. This dimensionless 1D advection – dispersion equation is solved using Laplace transform [6] to obtain eq. (2.5.4) below, describing the concentration of an injected fluid as a function of space and time [33].

$$C_D(x_D, t_D = \frac{1}{2}[erfc\left(\frac{x_D - t_D}{2\sqrt{\frac{t_D}{N_{Pe}}}} \right)] \tag{2.5.4}$$

2.5.1. 1D CONCEPTUAL ADVECTION DISPERSION EXPERIMENT

The analytical solution 2.5.4 of the one-dimensional advection-dispersion equation stated earlier 2.5.1, is used to plot the concentration in a one-dimensional conceptual reservoir in dimensionless form. This conceptual experiment is conducted in order to become familiar with the effect of changing the parameters in eq. (2.5.4). The result is shown in fig. 2.4, where the influence of the mentioned parameters is visualised. A high hydrodynamic dispersion results in a lower Peclet number, as it is found in its denominator 2.5.2. On the other hand, a high flow speed, meaning a high influence of advection, usually results in a higher Peclet number, as it is found in its numerator 2.5.2. However, the hydrodynamic dispersion coefficient also has a mechanical dispersion component, which is dependent on flow velocity. Therefore the flow speed only influences the Peclet number if D_e is around the same order of magnitude as D_m or higher. If D_e is much smaller than D_m, the effect of u_x in the numerator and denominator of the Peclet number will cancel out.

The plots in fig. 2.4 show a development of the one-dimensional mixing front over dimensionless time. The dimensionless concentration is plotted against the dimensionless position for a reservoir of length 1000m and porosity 0.1. All simulation parameter settings are displayed in table 2.1 The dispersivity is set to 50m [27] and the cementation factor is set to 1.0 [27]. As in most reservoirs of comparable length the flow velocity is a few meters per day [12], the flow speed is set to 2.32E-5 m/s. The left and right figure, both showing 10 time steps, were generated from a simulation with Peclet numbers of 199 and 41 respectively. The higher and lower Peclet number resulting from a hydrodynamic dispersion of 1.16E-3 m^2/s and 5.54E-3 m^2/s respectively. This implies that a low Peclet number, e.g., mixing with a higher influence of diffusion, results in a concentration which is more gradually decreasing through the reservoir for each moment in time. This can also be described as a larger mixing-zone.

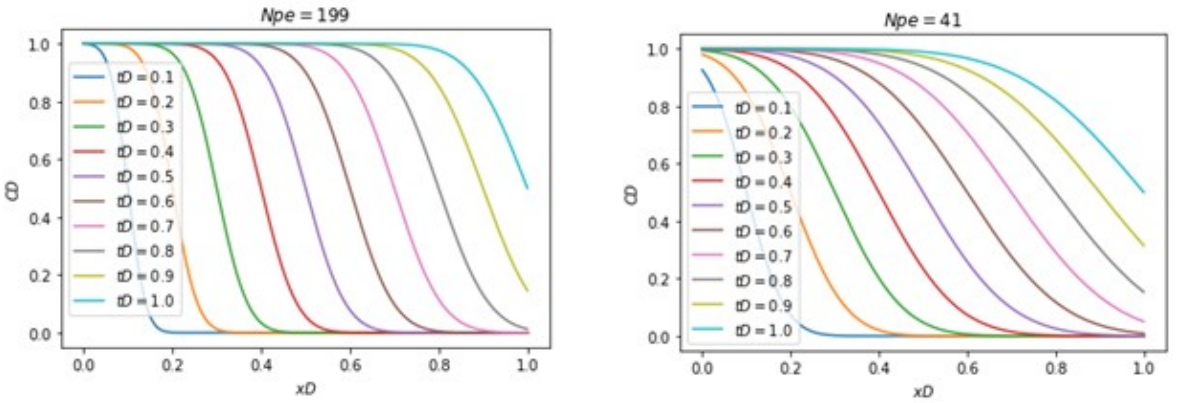

(a) High Peclet number, representing high ratio of advective over dispersive forces

(b) Low Peclet number, representing low ratio of advective over dispersive forces, causing a larger mixing zone

Figure 2.4: Dimensionless concentration plotted against dimensionless position at ten dimensionless time steps.

Table 2.1: Parameters used for generating the plots in fig. 2.4

Parameter	**Left figure**	**Right figure**
$u[m/s]$	2.32E-5	2.32E-5
ϕ	0.1	0.1
$L[m]$	1000	1000
$D_0[cm^2/s]$	4.38E-3	4.38E3
$D_e[cm^2/s]$	4.38E-5	4.38E1
$D_m[m^2/s]$	0.00116	0.00116
$D_h[m^2/s]$	0.00116	0.00554
m	2	3
$\alpha[m]$	50	50

Apart from obtaining theoretical insight into simulations that will later be done in CMG GEM, the reason for simulating simplified analytical solutions is to compare potential cushion gases for hydrogen storage. In the 1D simplified test setup from fig. 2.4, CH_4 (Methane), CO_2 (Carbon-dioxide), and N_2(Nitrogen) are considered as initial cushion gases. Consequently, H_2 is injected into the reservoir and the mixing front is plotted for dimensionless time step 0.5. During this simulation, three scenarios with conditions of constant pressure and temperature are considered as shown table 2.2 The mixing zone is defined as the reservoir distance between a concentration of 0.9 and 0.1, which is calculated with eq. (2.5.5) below [33].

$$\Delta X_D = 3.625\sqrt{\frac{t_D}{N_{Pe}}} \tag{2.5.5}$$

The different cushion gases are represented by the corresponding diffusion coefficient D_0, which for each of them is calculated at the 3 different scenarios through eq. (2.5.6) [34]. Consequently D_e is calculated through eq. (2.3.1), which is shown in table 2.2.

$$D_0 = \frac{AT^{\frac{3}{2}}\sqrt{\frac{1}{M_1}+\frac{1}{M_2}}}{p\sigma_{12}^2\Omega} \tag{2.5.6}$$

Table 2.2: Showing 3 scenarios of constant pressure and temperature where the mixing zone is calculated for 3 different cushion gases in combination with hydrogen through a 1D simulation. Al simulations have a constant flow speed $u = 0.1 ms^{-1}$ and reservoir length of 10m. Al mixing zones are calculated at dimensionless time step 0.5

	Gas composition	D_0 **[cm^2/s]**	**Peclet number**	**Dimless. Mixing zone**	**Mixing zone [m]**
Scenario 1	H_2-CH_4	8.8E-3	200	0,18125069	1.81250687
[100 Bar,	H2-CO2	8.0E-3	200	0,18125062	1.81250625
70 °C]	H2-N2	8.9E-3	200	0,18125070	1.81250695
Scenario 2	H_2-CH_4	6.2E-1	200	0,18129843	1.81298431
[1 Bar,	H2-CO2	5.7E-1	200	0,18129453	1.81294526
0 °C]	H_2-N_2	6.3E-1	200	0,18129921	1.81299212
Scenario 3	H_2-CH_4	4.4E-3	200	0,18125034	1.81250344
[200 Bar	H2-CO2	4.0E-3	200	0,18125031	1.81250312
90 °C]	H_2-N_2	4.5E-3	200	0,18125035	1.81250352

In order to learn something about the differences between the cushion gases from this simulation, the mixing zones of the three different gas compositions should be compared for each of the conditions. The mixing zone column of table 2.2 shows that at typical reservoir conditions (scenario 2), the mixing zone lengths for the different cushion gas-H_2 combinations are almost identical. The difference between H_2-CH_4 and H_2-N_2 is within the order of E-7 meters. fig. 2.5 shows the dimensionless concentration against dimensionless position for the three different cushion gas combinations at time step 0.5. The red-dotted lines are the boundaries of 0.9 and 0.1 dimensionless concentration between which the mixing zone is defined. The difference between the three plots cannot by eye be distinguished. The conclusion of this simulation and the calculations is that for a one-dimensional system, where the flow speed and hydrodynamic dispersion are assumed constant, the influence of effective molecular diffusion is negligible compared to advection and mechanical dispersion.

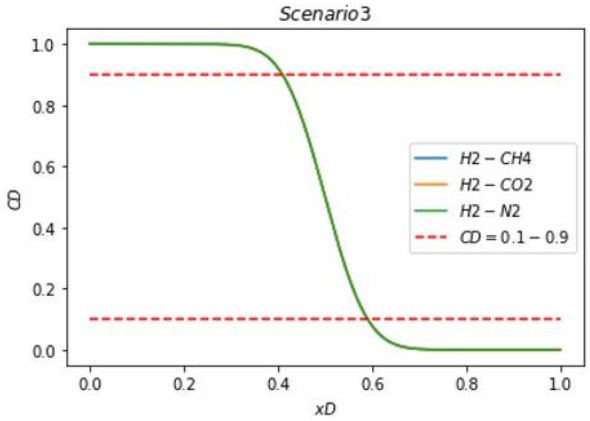

Figure 2.5: Displaying difference in mixing zones (not visible) for different gas combinations during 1D-simulation at 200 bar, 70 Celsius, 0.1 ms^{-1}, $\phi = 0.1$, L = 10m. Red lines show the 0.1 and 0.9 dimensionless concentration levels between which the mixing zone is defined.

2.6. 2D-RADIAL ADVECTION & DISPERSION

In order to compare a 2D-radial system to the earlier analyzed 1D system for hydrogen gas injection, the divergences in eq. (2.2.1) should be simplified. The term $\phi \frac{\partial C}{\partial t}$ is already in the desired form. For the full derivation see appendix A. A 2D radial system is assumed, which is homogeneous at the reservoir scale and where the flow velocity is decreasing as the injected gas propagates outward. However, the flow velocity and concentration are assumed equal at all angles θ and there is no z-component as we are observing a 2D system. Simplifying eq. (2.2.1), leads to eq. (2.6.1).

$$\phi \frac{\partial C}{\partial t} + \left(u_r - \frac{\phi D_h}{r} - \phi D_h - \frac{\phi \partial D_h}{\partial r} \right) \frac{\partial C}{\partial r} + \frac{C \partial u_r}{\partial r} - \phi \frac{D_h \partial^2 C}{\partial r^2} - \phi \frac{\partial C}{r} \frac{\partial D_h}{\partial r} + \frac{r C u_r - \phi D_h C}{r^2} = 0 \tag{2.6.1}$$

Equation (2.6.1) contains six main terms, five of which contain a partial differential equation. In order to

better understand the effect of $\frac{\partial u_r}{\partial r}$ and $\frac{\partial D_h}{\partial r}$, they are separately analyzed below. The following definitions for u_r and D_h are known:

$$\frac{\partial A}{\partial t} = \frac{\partial A}{\partial r}\frac{\partial r}{\partial t}, \qquad \frac{\partial A}{\partial t} = 2\pi r \frac{\partial r}{\partial t}, \qquad \frac{\partial r}{\partial t} = \frac{\partial A}{\partial t}\frac{1}{2\pi r} \qquad u(r) = \frac{q}{2\pi r}, \qquad \longrightarrow \frac{\partial u_r}{r} = \frac{-q}{4\pi r^2}$$

In the definitions above q is the injection rate $\frac{\partial A}{\partial t}$ in $m^2 s^{-1}$, and $\frac{\partial r}{\partial t}$ is the velocity of the propagating injected fluid. The r^2 in the denominator of the negative $\frac{\partial u_r}{\partial r}$ term in eq. (2.6.1) means that the fluid flow velocity decreases in an inverse exponential way. The flow velocity increases exponentially when approaching the injection location, which is in the center of the radial system. This is visualized in fig. 2.6, where a two-dimensional injection rate of 0.01 $m^2 s^{-1}$ was used.

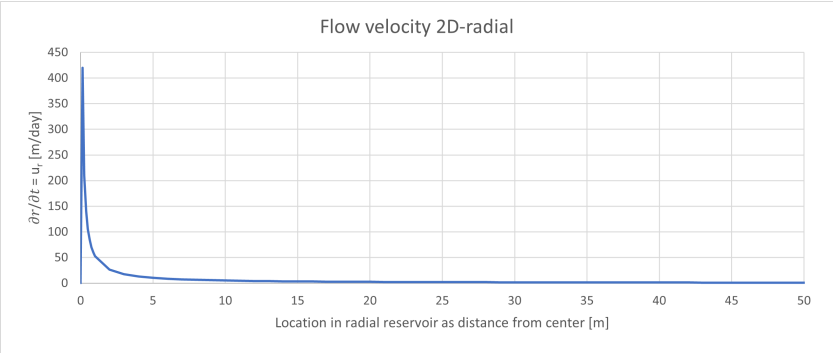

Figure 2.6: The flow velocity of the injected fluid shows a reversed exponential decay, where the flow decreases most rapidly close to the well and relatively slowly far from the well.

$$D_h = \alpha u + D_0 \phi^m = -\alpha \frac{q}{2\pi r} + D_0 \phi^m \longrightarrow \frac{\partial D_h}{\partial r} = \frac{-\alpha q}{4\pi r^2}$$

Table 2.3: Comparing contributions of D_e and D_m to D_h at different radii from injection well.

Radius [m]	$D_e[m^2/s]$	$D_m[m^2/s]$
1	4.4E-8	5.83E-2
500	4.4E-8	1.16E-4
1000	4.4E-8	5.83E-5
10000	4.4E-8	5.83E-6

Because the effective diffusion $D_0\phi^m$ is a constant, it is not influenced by the location in the reservoir, as shown in table 2.3. The Mechanical dispersion D_m however is a variable dependent on $u(r)$ and therefore on the location in the reservoir r. As $\frac{\partial D_h}{\partial r} = \frac{-\alpha q}{4\pi r^2}$, which also has r^2 in its denominator, the dispersion decreases with the same factor as the flow velocity. The decrease of dispersion in a two-dimensional radial system is shown in fig. 2.7.

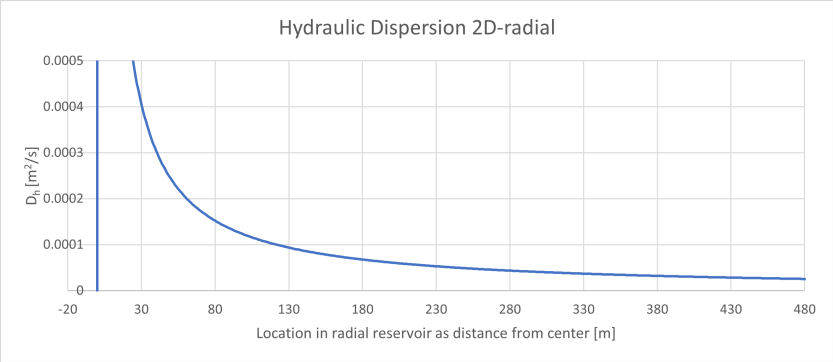

Figure 2.7: The hydrodynamic dispersion of the injected fluid shows a reversed exponential decay, where the flow decreases most rapidly close to the well and relatively slow far from the well.

From analyzing the dispersion and flow velocity, it becomes clear that the effective molecular diffusion has a negligible contribution to the concentration close to the well and still a relatively small contribution further away from the well. table 2.3 compares the contribution of D_e, and D_m to D_h, for the conditions shown in table 2.4.

Table 2.4: Parameters used for fig. 2.6, fig. 2.7, and table 2.3. Flow rate q is based on a rate of 5E+6 Nm^3/day, which is considered as 2D by dividing through an assumed reservoir thickness of 50m.

Parameter	**Value**
P[bar]	200
T[°C]	70
D_0[cm^2/s]	4.4E-3
m	1
ϕ	0.1
$\alpha[m]$	50
$u_r[m/s]$	$q/\pi 2r$
q[m^2/s]	0.00733

In the dimensionless advection dispersion equation 2.5.2 the concentration within the reservoir is dependent on the Peclet number, which in turn is dependent on the dimensionless time and location and the advective and dispersive forces, of which the latter two are constant due to the assumed constant flow speed. This means that for the one-dimensional system, concentration gradient is constant and the mixing front moves stable and at constant speed through the reservoir. In the two-dimensional advection equation, the concentration is dependent on a combination of variables, almost all of which are related to Dh and Ur and therefore dependent on the radius r. The effective molecular diffusion (D_e) part of hydraulic dispersion (D_h) is not dependent on the reservoir radius (r), which is shown in table 2.3. It is relatively complicated to find a solution to the two-dimensional advection-dispersion equation. However, because the spatial behavior of the variables in its simplified form is known, it is possible to make a qualitative description of the concentration distribution through the 2-D radial system.

2.7. 3D-RADIAL ADVECTION & DISPERSION

In a 3D-radial system, where homogeneity is assumed at the reservoir scale, the $\frac{\partial C u_z}{\partial z}$ term, which results from simplifying the divergence in equation 1 for radial systems, can not be neglected. With the product rule for derivatives, $\frac{\partial C u_z}{\partial z}$ is simplified to $\frac{C \partial u_z}{\partial z} + \frac{u_z \partial C}{\partial z}$. The main difference between 2D and 3D radial systems is the $\frac{\partial u_z}{\partial z}$ factor caused by gravity. The effect of gravitational force on the gas components in the reservoir depends on the difference in density of the gas components. However, the gravitational force is relatively low compared to advective forces close to the injection well. Further away from the injection well, mechanical dispersive forces are more dominant together with gravitational force, depending on the density difference between gas components. At a large distance from the injection well, diffusive forces may become relatively influential on the mixing behavior during longer periods of storage. Furthermore, the more-dimensional system causes the overall process of of fluid flow and mixing to be influenced by heterogeneities and anisotropies of the porous

medium.

2.8. NUMERICAL DISPERSION

In order to numerically analyze the outcome of the advection-dispersion equation 2.2.1, it has to to be discretized over grid blocks with a certain size. Consider a simplified form of the advection-dispersion equation below, without any hydrodynamic dispersion [23]. The concentration of a component in single fluid phase is represented by C, and flow velocity u is assumed to be constant.

$$-u\frac{\partial C}{\partial x} = \phi\frac{\partial C}{\partial t}$$

In order to obtain the difference analog of the modified form of eq. (2.2.1) above, its temporal and spatial derivatives should be approximated. The spatial derivative equation is given in eq. (2.8.1)[23].

$$\frac{\partial C}{\partial x} = \frac{C_{i+1/2} - C_{i-1/2}}{\Delta x} \tag{2.8.1}$$

A visualization of the grid block indices for the system under consideration is given in fig. 2.8. The concentrations are only available at the center of the grid blocks, and therefore $C_{i+1/2}$ and $C_{i-1/2}$ need to be evaluated in terms of those values. There is a variation of possibilities to define the concentration at the cell borders, giving rise to different weighting schemes [35] such as: upstream weighting, mid-point weighting, and downstream weighting. Upstream weighting equals the concentration at cell border $i-1/2$ to that of upstream cell $i-1$. Downstream weighting equals the concentration at cell border $i-1/2$ to that of downstream cell i. Midpoint weighting equals the concentration at cell border $i-1/2$ to half the concentration at cell $i-1$ added to half the concentration at cell i.

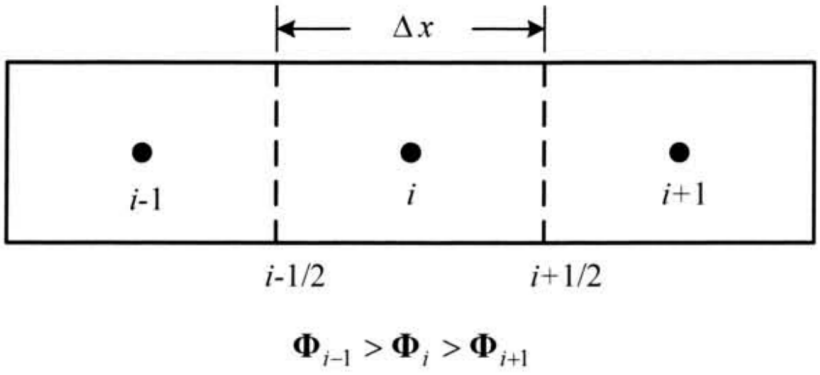

Figure 2.8: Discretization of a linear system showing block indices and the downstream direction. Where, $\Phi = potential$ decreasing from left to right

A similar approach can be followed towards differentiating among explicit, implicit and centered-in-time difference equations. If θ is chosen as the time-weighing parameter, then eq. (2.8.1) can be replaced by eq. (2.8.2). where, $\theta = 1$ results in implicit calculation, $\theta = 1/2$ results in centered-in-time calculation, and $\theta = 0$ results in explicit calculation of the concentration at the grid block boundaries [23].

$$-\frac{u}{\Delta x}\left[\theta\left(C^{n+1}_{i+1/2} - C^{n+1}_{i-1/2}\right) + (1-\theta)\left(C^{n}_{i+1/2} - C^{n}_{i-1/2}\right)\right] = \phi\frac{C^{n+1}_i - C^n_i}{\Delta t} \tag{2.8.2}$$

Numerical dispersion is in fact the truncation error that results from the simulator describing the concentration at the grid block boundary in terms of the concentration at the grid block centers. To carry out a truncation error analysis, Taylor series expansion can be done about C^n_i for both spatial and temporal differences [23]. This Taylor expansion calculation leads to the numerical dispersion description in eq. (2.8.3)

$$D_{num} = \left(\frac{u}{\phi}\right)\frac{\Delta x}{2} \tag{2.8.3}$$

where the following boundary condition is required:

$$\frac{u\Delta t}{\phi} << \Delta x$$

This means that the numerical dispersion in a linear system is equal to half of the grid cell size. In order for this to be true, flow velocity and time step size need to be such that in one time step, the front does not advance beyond a grid-lock length. [23]

2.9. HIGHER ORDER METHOD FOR NUMERICAL DISPERSION CONTROL

Higher order upstream weighting schemes are numerical modelling methods which are used to reduce numerical dispersion [23]. They are based on the idea of incorporating extra grid-points of neighbouring cells in the discretization, enabling more accurate calculation of the concentrations at the cell borders, with less front smearing 2.8. The GEM simulator, used in this thesis, is able to run in a numerical disperion control mode which uses higher order schemes under a Total Variation Diminishing (TVD) flux limiter [34]. TVD methods are algorithms that ensure that the local variation of flow variables does not increase with time, thus no excessive oscillations are generated [23]. In other words, the TVD flux limiter helps to keep the numerical calculations stable when the higher order upstream weighing schemes are applied. The keyword used in GEM to activate the explained method of numerical dispersion control is *TWOPTFLUX.

2.10. GRAVITATIONAL SEGREGATION

Gravitational segregation is a physical phenomenon taking place due to a difference in density and mobility of multiple fluid components that are in contact with each other. The less dense fluid will tend to displace the denser fluid in the upper part of the reservoir [36]. In more applied terms; a relatively low density displacing fluid being injected into a structure which is filled by a denser displaced fluid, would tend to rise on top of the the displaced fluid. This process is called gravity override or gravitational segregation. The isothermal densities of hydrogen and methane are plotted against pressure for a range of temperatures in fig. 2.9a, clearly showing a large density difference with the potential for gravitational segregation

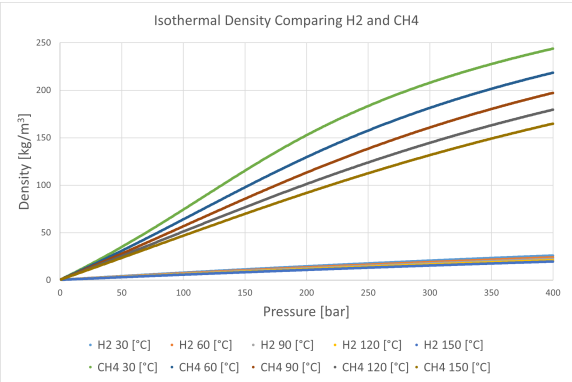

(a) Isothermal densities of H_2 and CH_4 plotted against pressure for a range of temperatures from 30 $^\circ C$ up to 150$^\circ C$

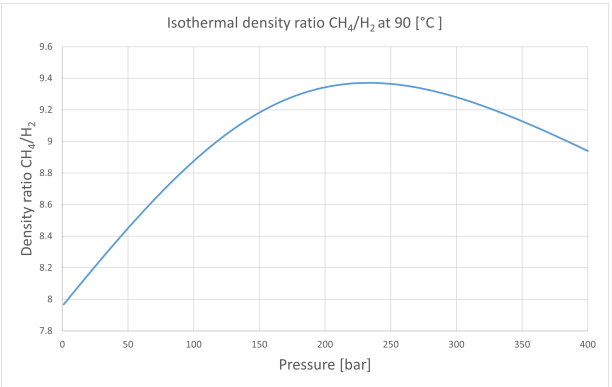

(b) Density ratio between CH_4 and H_2 at 90$^\circ C$

Figure 2.9: Plots comparing the isothermal densities of hydrogen and potential cushion gas methane.

It is shown in fig. 2.9 that the density ratio between methane and hydrogen at 90 $^\circ C$ is between roughly 8 and 9.5 for pressures up to 400 bar. This naturally leads to a large gravitational segregation potential when injecting hydrogen into a methane filled reservoir. fig. 2.9a shows that the density of both methane and hydrogen increase with pressure. However, the density of methane increases by a larger factor than that of hydrogen if the pressure is increased. Therefore, the density ratio between the two gasses is increasing at higher pressure, which accommodates a larger potential for gravitational segregation. For both gases, the density increases at lower temperatures.

This research focuses on gas-gas interaction. The ratio of gravitational over viscous forces during the transport of gases in porous media is quantified by eq. (2.10.1), in which N is defined as the gravity number [37]

$$N = \frac{k_v \Delta\rho g \rho_c 2\pi r_c d}{k_h \mu_{H2} Q_m} \tag{2.10.1}$$

In this equation, k_v and k_h are the vertical and horizontal permeability values, $\Delta\rho$ is the density difference between the fluids, r_c is the radius of the reservoir, d is the reservoir thickness, μ_{H2} is the viscosity of H_2, and Q_m is the mass flow rate. ρ_c is the characteristic density, which can be taken as the mean of the injected H_2 volume. The miscible gas flow regime is dominated by gravitational forces for cases where $N >> 1$, and dominated by viscous forces for cases where $N << 1$.

2.11. VISCOUS FORCES

The analytical approach in eq. (2.10.1) however, neglects the viscosity of the displaced fluid. The isothermal viscosity of hydrogen and methane at various temperatures in the range of 30 $^\circ C$ to 150 $^\circ C$ is displayed in fig. 2.10a. It is visible that the viscosity of methane is increasing with pressure, where that of hydrogen is not. The ratio between the isothermal viscosities of methane and hydrogen at a temperature of 90 $^\circ C$ is displayed in fig. 2.10b. It is visible that the ratio between the viscosities of methane and hydrogen increases with pressure, which is a destabilizing factor during the injection of hydrogen in a methane filled reservoir.

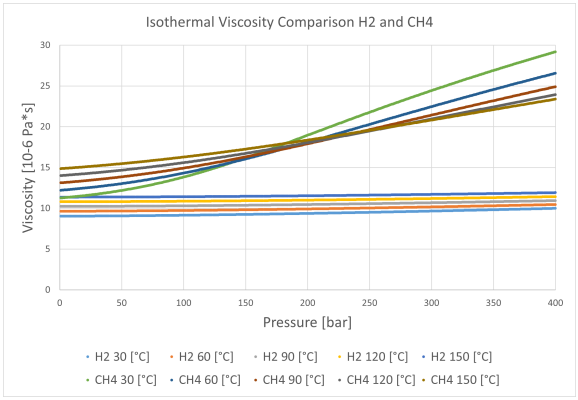

(a) Isothermal viscosity of H_2 and CH_4 plotted against pressure for a range of temperatures from 30°C up to 150°C

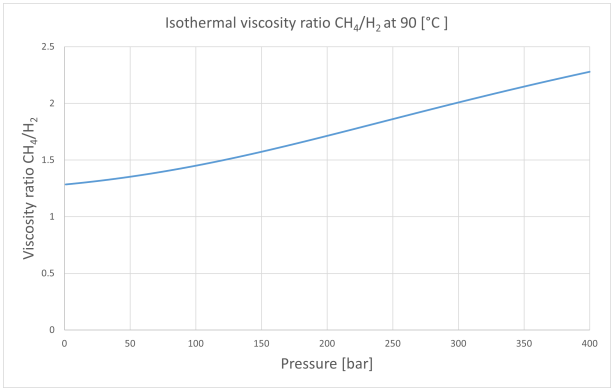

(b) Viscosity ratio between CH_4 and H_2 at 90°C

Figure 2.10: Plots comparing the isothermal viscosity of hydrogen and methane.

In eq. (2.11.1), both density and viscosity of the displacing and the displaced fluid are taken into account. This leads to the parameter $\gamma_{g_{inj},g_{res}}$, describing the relative importance of gravitational over viscous forces [38].

$$\gamma_{g_{inj},g_{res}} = \frac{k_v 2\pi d^2 g}{k_h Q_0} \frac{\Delta\mu}{\Delta\rho} \tag{2.11.1}$$

In which Q_0 is the volumetric flow rate in Nm^3/s. k_v and k_h are the vertical and horizontal permeability values. For $\gamma_{g_{inj},g_{res}} < 0$, a less dense fluid displaces a more dense fluid, and visa versa for $\gamma_{g_{inj},g_{res}} > 0$. For values $0 < \gamma_{g_{inj},g_{res}} < 1$, gravitational forces are dominant during the displacement process. For $\gamma_{g_{inj},g_{res}} << 1$, the displacement process is dominated by viscous forces.

3 | Modeling Approach

The main objective for this research is to make predictions about the mixing behaviour of hydrogen in combination with a (residual) cushion gas in a subsurface reservoir. In order to answer the research questions, a step-wise approach with alternating stages of reservoir simulations and result analysis is conducted. For this study it is important that fluid interaction between different gas components is realistically calculated because the focus is on UHS in gas reservoirs instead of aquifers. This means that miscibility, variable density and viscosity need to be incorporated in the used modelling software. The reason for using reservoir simulation is to be able to make predictions about the hydrodynamic behaviour of hydrogen in the reservoir and to visualize the processes that take place.

3.1. GEM RESERVOIR SIMULATOR & GOVERNING EQUATIONS

The simulation software used in this study is 'GEM' from the Computer Modelling Group (CMG) [34]. GEM is a multidimensional, equation-of-state (EOS), compositional simulator, which has the ability to simulate all important mechanisms of the miscible gas injection and production processes. In hydrocarbon related reservoir simulation GEM is used for vaporization and swelling of oil, condensation of gas, viscosity reduction, interfacial tension reduction, and the formation of a miscible solvent bank through multiple contacts [34]. GEM has the capability of running fully implicitly, which is a feature that is also required for miscible gas simulations related to dispersive processes and high flow rates near the injector well (radial system). Another feature in the GEM simulator is the option to simulate mechanical dispersion and effective molecular diffusion, whereas in most other reservoir simulators, only numerical dispersion is incorporated [21]. The multi-component, miscible simulation capabilities in which variable gas viscosity and densities are incorporated as well as the option for fully implicit calculations including physical dispersion, make GEM a highly suitable reservoir simulator for this thesis research. During the reservoir simulations, the gas density is calculated from the Peng-Robinson equation of state [39]. The gas viscosity is estimated from the Jossi, Stiel and Thodos correlation [26]. The material balance fluid flow of component i and phase m is defined by [40] eq. (3.1.1)

$$\frac{\partial}{\partial t}\left(\phi \sum_{m=1}^{n_p} \rho_m S_m C_{im}\right) = \sum_{m=1}^{n_p} \nabla k \rho_m \lambda_m C_{im}(\nabla p_m - \rho_m g \nabla d) + \sum_{m=1}^{n_p} \nabla \alpha_m |\vec{v}_m| \rho_m \nabla C_{im} \tag{3.1.1}$$

The term after the summation sign in the right part of eq. (3.1.1) is responsible for hydrodynamic dispersion. From this point onward in the report, hydrodynamic dispersion is called by its other name 'physical dispersion' because it is clearer when comparing it to numerical dispersion. The dispersion is assumed to be longitudinal dispersion only because of the negligible influence of the transversal dispersion [3]. The dispersion term is dependent on the dispersivity and the fluid flow velocity. The discretized material balance fluid flow equation is given in eq. (3.1.2).

$$\Psi_i = \Delta T_g^u y_{ig}^u (\Delta p^{n+1} + \Delta P_{cwg}^u - \rho_g^u g \Delta d) + \Delta T_w^u y_{iw}^u (\Delta p^{n+1} - \rho_w^u g \Delta d) + \sum_{q=g,w} \Delta D_{iq}^u \Delta y_{iq}^u \qquad i = 1, ..., n_c \tag{3.1.2}$$

(For list of abbreviations see the third page of this document.)

In eq. (3.1.2), the superscripts u and n+1 represent explicit and implicit calculation, respectively. The term after the summation sign in the right part of eq. (3.1.2) is responsible for physical dispersion. Everything before the summation sign, which is all dependent on the pressure gradient, describes advection. Notice that the intra-aqueous reaction rates and mineral dissolution/precipitation rates are not taken into account in this equation. The transmissibility is defined by Cordazzo *et al.* 2002 [41] through eq. (3.1.3).

$$T = \frac{\lambda \sqrt{\alpha}}{\Delta n} \tag{3.1.3}$$

In eq. (3.1.3), λ is the mobility, which is defined in [41]as eq. (3.1.4). α is a geometric grid angle, and Δn is

the distance between two grid points.

$$\lambda = \frac{kk_r}{B\mu} \tag{3.1.4}$$

K and k_r are the intrinsic and relative permeability values respectively, and B is the formation volume factor. As displayed by eq. (3.1.4), the mobility is dependent on the fluid viscosity, making it different for a potential cushion gas and hydrogen in a storage reservoir. This causes the flow velocity for gas mixtures with different mole fractions to vary, contributing to the mixing zone.

Flow velocity modeled by the GEM reservoir simulator is computed through Darcy's law eq. (3.1.5). [34]

$$u_k = -\left(\frac{kk_{r,k}}{\mu_k}\right)(\nabla p + \nabla P_{c,k} - \rho_k g \nabla d) \tag{3.1.5}$$

3.2. WORKFLOW

In order to access the CMG GEM software licence provided by TUDelft, a VPN connection is established through Forticlient VPN. The workflow used to obtain simulation outputs in the desired format, is a combination of Excel (including Visual Basic), CMG GEM, CMG Results, and Tibco Spotfire (fig. 3.1). Each of the steps in the workflow is explained below:

1. The workflow starts in Excel, which is in this step used to create a table with input parameters for simulations that are to be executed. This same table is used as a database to store the input parameters of all simulations that have been and are to be executed, which are mostly modifications to the base case of section 3.3.

2. Visual Basic is used to generate a new Excel tab, into which the values from the input table are inserted in the desired format to be read by CMG GEM. Consequently, the Visual Basic script saves this new tab as a .dat file, which is a file type that can be read by CMG GEM.

3. In this step, the .dat file generated in step 2 is manually opened and run in CMG GEM. After which CMG GEM generates a .log file, that contains information about any running errors, and a .sr3 file, containing the simulation results, which can be opened with CMG Results.

4. CMG Results is used to open the generated .sr3 file and to obtain some first impressions on the simulation result. This software enables (3D) visualization of the simulation over time, and simple plots of well' and field data. However, for more complicated output data, such as the produced hydrogen volume before a purity or rate threshold is reached, CMG Results is not adequate.

5. In order to calculate more complex characteristics from the simulation results, as the one mentioned in step 4, a list of output parameters is exported from CMG Results to Excel.

6. Now that the most important output parameters are exported to Excel, another Excel Visual basic script is run to calculate all desired characteristics from the simulation results.

7. Finally, the Excel output table is loaded into Tibco Spotfire, where the data can be extensively analyzed and visualized in plots showing multiple parameters simultaneously.

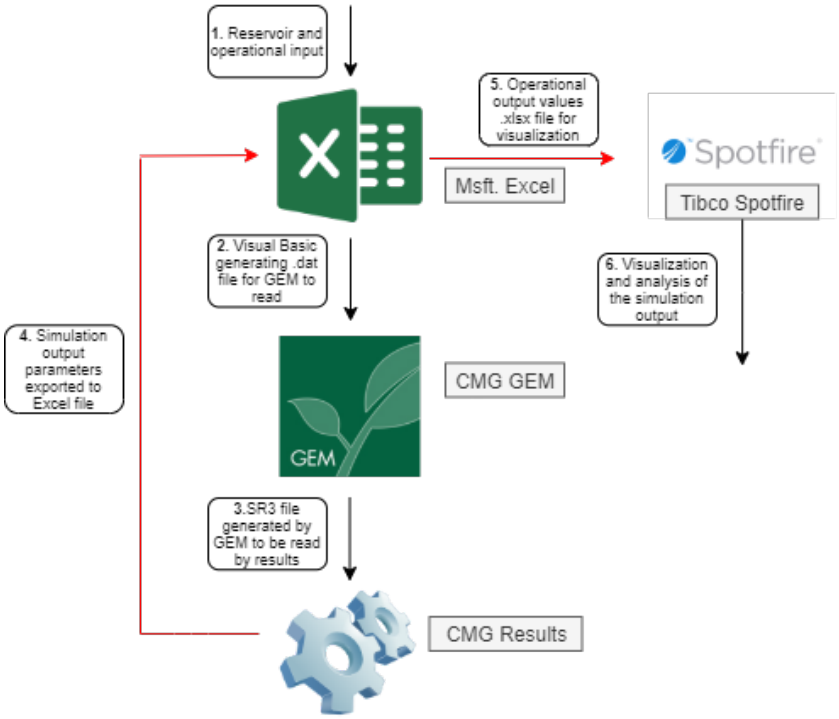

Figure 3.1: Software workflow visualization

3.3. BASE CASE CONCEPTUAL RESERVOIR MODELING

The radial reservoir model as shown in fig. 3.2 is constructed in CMG BUILDER, which is part of the same software package as GEM. BUILDER has an interface which helps the user to first create a geometric framework of the reservoir model and consequently set all parameters ranging from the initial reservoir conditions, well types and settings, rock fluid types, to reservoir fluid types and operating schemes. The created radial model is used as a base case for the reservoir simulation experiments in this thesis. The characteristics of the model are mostly the same for all experiments. However, depending on the purpose of each experiment, some reservoir' and operating parameters deviate from the base case. The conceptual reservoir is a 3D radial reservoir, with porous medium properties (see table 3.1) based on typical Dutch sandstone reservoirs [5], which are assumed homogeneous and isotropic for simplicity of the experiments. The initial reservoir pressure of a natural gas field before injecting hydrogen could, depending on the depth, range anywhere from completely depleted pressure of roughly 15 bar to partly depleted pressures of more than 200 bar [42]. The temperature is set to 90 $^{\circ}C$, because the temperature at the base of the Dutch Zechstein salt, which functions as a cap rock for most of the gas fields, ranges from 70 $^{\circ}C$ to 110 $^{\circ}C$ [5]. A temperature map of the Zechstein base in the Netherlands can be found in the appendix fig. C.3. The maximum production and injection rates are taken as 10E+6 and 5E+6 Nm^3 per day respectively, which is within the boundaries that are stated as rate capacities of the current Dutch UGS fields [43]. As mentioned in section 3.3, the reservoir characteristics like porosity, permeability and water saturation are based on typical Dutch sandstone reservoirs.

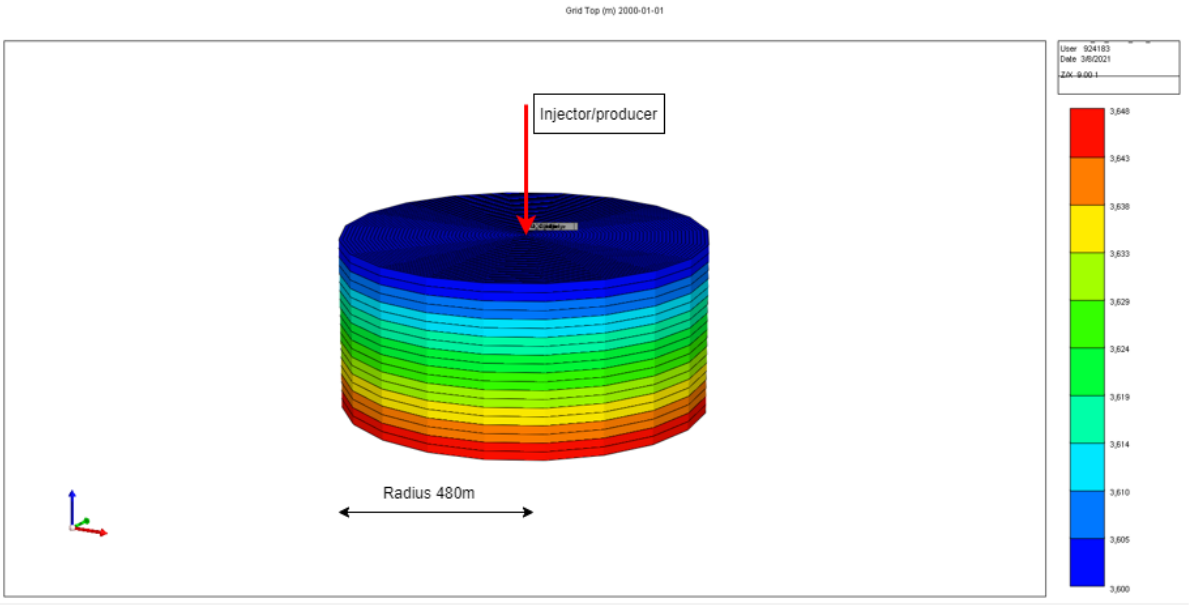

Figure 3.2: Base case conceptual radial model in GEM reservoir simulator. Color scale in this case displays reservoir depth (TVD)

Table 3.1: Conceptual model (base case) reservoir parameters

Reservoir parameters	**Value**	**Unit**
Reservoir radius	480	[m]
Reservoir thickness	50	[m]
Number of cells in i/j direction	48	[-]
Number of cells in k direction	20	[-]
Time step size	0.2	[s]
Location injection well	Center	[-]
Location production well	Center	[-]
Max. injection rate	5.0E+6	[Nm^3/day]
Max. production rate	1.0E+7	[Nm^3/day]
Porosity	0.12	[-]
Permeability	20	[mD]
Effective molecular diffusion	4.46E-5	[cm^2/s]
Longitudinal Dispersivity	1	[m]
K_i/K_k	0.1	[-]
Connate water saturation	0.15	[-]
Reservoir temperature	90	[°C]
Reservoir top depth	3600	[m]
Initial reservoir gas	CH_4	[-]
Initial reservoir pressure	200	[Bar]
Target inj. reservoir pressure	360	[Bar]
Rate constraint	3.0E+6	[Nm^3/day]
Purity constraint	0.99	[Mole frac. H_2 of produced gas]

4 | Gravitational segregation

Gravitational segregation, the principles of which have been discussed in section 2.10, is a process that could potentially cause hydrogen losses during UHS operations in gas fields. If the lighter hydrogen molecules rise over heavier cushion gas molecules like methane, they could end up in a location in the reservoir from where they are unlikely to be produced before mixing with the cushion gas. In order to see what effect gravitational segregation has on the recoverable volume-fraction of hydrogen, and under what conditions gravitational segregation arises most significantly, some basic reservoir and operational parameters are varied on the base case conceptual model from section 3.3. The specifications of the experiment are described below in section 4.1

4.1. Objectives and methodology

For the simulations in this chapter, the following objectives are set in order to move towards answering the corresponding sub research question:

- Analyzing the effect of permeability on the first storage cycle characteristics for a high volume of H_2 compared to the CH_4 cushion gas.
- Analyzing the effect of increasing the initial amount of CH_4 cushion gas. The same reservoir permeability values are tested as for the first objective.
- Analyzing the effect of varying the reservoir dimensions on the first storage cycle characteristics for both amounts of initial CH_4 cushion gas in the reservoir.

In order to achieve these objectives, the base case setup of table 3.1 is used. Variations on this base case were made in terms of permeability, reservoir radius, reservoir thickness, and the initial volume of CH_4 cushion gas in the reservoir, to determine their influence on recoverable hydrogen volume fraction for the first storage cycle. When adjustments are made to the reservoir dimensions in this experiment, the grid cell size is kept constant. This keeps numerical dispersion, explained in section 2.8 constant, preventing it from influencing the results. For this experiment, mixing is caused by numerical dispersion instead of physical dispersion. The reason for this choice is that there is no experience with the physical dispersive option of the simulator at this point in the research, and for quantification of gravity segregation between the initial and injected gas the exact magnitude of the mixing zone is not as important. The analysis on the amount of gravitational segregation is conducted on the the bulk volume of the hydrogen and cushion gas rather than the mixing zone 2.5.1.

Table 4.1: Parameters used for simulating gravity effect as a results of permeability and reservoir dimensions. Deviations from base case are written in bold

Changed Variable	Permeability		Perm + Thickness		Perm + Radius		Perm + Thickness	
Simulation Set #	**1.1**	**1.2**	**2.1**	**2.2**	**3.1**	**3.2**	**4.1**	**4.2**
Radius [m]	480	480	480	480	**960**	**960**	480	480
Thickness [m]	50	50	**25**	**25**	50	50	**25**	**25**
Nr. of gridcells i	48	48	48	48	**96**	**96**	48	48
Nr. of gridcells k	20	20	**10**	**10**	20	20	**10**	**10**
K_z/K_i	0.1	0.1	0.1	0.1	0.1	0.1	0.1	0.1
Inj. rate max.[Nm^3/day]	5.0E+6	5.0E+6	5.0E+6	5.0E+6	5.0E+6	5.0E+6	5.0E+6	5.0E+6
Prod. rate max. [Nm^3/day]	1.0E+7	1.0E+7	1.0E+7	1.0E+7	1.0E+7	1.0E+7	1.0E+7	1.0E+7
Min BHP prod. [bar]	60	60	60	60	60	60	60	60
Permeability Ki [mD]	**10, 50, 200, 500**	**10, 50, 200, 500**	**10, 50, 200, 500**	**10, 50, 200, 500**	**10, 50, 200, 500**	**10, 50, 200, 500**	20, **100, 400, 1000**	20, **100, 400, 1000**
Initial gas in reservoir	CH_4	CH_4	CH_4	CH_4	CH_4	CH_4	CH_4	CH_4
Injected gas	H_2	H_2	H_2	H_2	H_2	H_2	H_2	H_2
Initial res. pressure [bar]	**40**	200	**40**	200	**40**	200	**40**	200
Final inj. pressure [bar]	360	360	360	360	360	360	360	360
Timestep [day]	0.1	0.1	0.1	0.1	0.1	0.1	0.1	0.1

4.1.1. SIMULATION DETAILS

This section provides more details on table 4.1 and the setup of the experiment. The first row of the table depicts the simulation set number, which has a first digit ranging from 1 to 4, and a second digit which is either 1 or 2. The first digit stands for the type of parameter that was varied during that specific experiment, where 1, 2, 3 and 4 are perm, perm + thickness, perm + radius, and perm + thickness (with double perm compared to 1) respectively. The second digit of the simulation set represents one of two initial pressures of the methane filled reservoir, where 1 corresponds to 40 bar initial reservoir pressure and 2 corresponds to 200 bar initial reservoir pressure. Each of the simulation numbers has 4 different runs corresponding to 4 different permeability values of 10, 50, 200, and 500 mD. In each simulation, pure hydrogen gas is injected in the center reservoir until the pressure reaches 360 Bar. Consequently, production will start from the center of the reservoir until one of the production constraints is reached, which are set as below:

1. Hydrogen mole fraction of the produced gas should be maintained above 98%
2. Production rate of produced gas should be maintained above 3 million Nm^3/day

Depending on the parameters, different simulation runs need different running times before one or both of the production constraints is reached. The running time varies from a few months to a few years.

4.2. RESULTS

In this section, the results of section 4.1 are presented. In order to transmit the result data in the most comprehensible and informative way to the reader, both plots and visualisations are used. The plots show the recoverable fraction of the injected hydrogen volume on the y-axis as a function of horizontal permeability on the x-axis. Furthermore the plots present which of the production constraints (mole fraction or rate) was first reached upon recovery of the gas, indicated by squared and circular data points respectively. The plots are grouped in multiple figures in order to compare both the effect of reservoir dimensions and the effect of the amount of hydrogen injected. The visualizations of the results show a 2D ($i * k$) cross section of the reservoir, in which the mole fraction of hydrogen is displayed. The result of each of the simulations specified in table 4.1 is visualized by two figures, each displaying a moment of time in the simulation. The two figures of each simulation are be separated by an arrow. The figure before the arrow, displays the moment of final hydrogen injection, e.g, 360 bar reservoir pressure. The figure after the arrow displays the moment at which the volume of recovered gas is 77.5% of that of the injected hydrogen. This way, all simulation runs can appropriately be compared. The visualised moment at 77.5% is displayed independent on the rate and purity constraints described in section 4.1.1.

4.2.1. VISUALIZATION RESULTS OF SIMULATION SETS 1.1 AND 1.2

In this section, the visualizations announced in section 4.2 are presented. These visualizations are shown in fig. 4.1, fig. 4.2, fig. 4.3, and fig. 4.4.

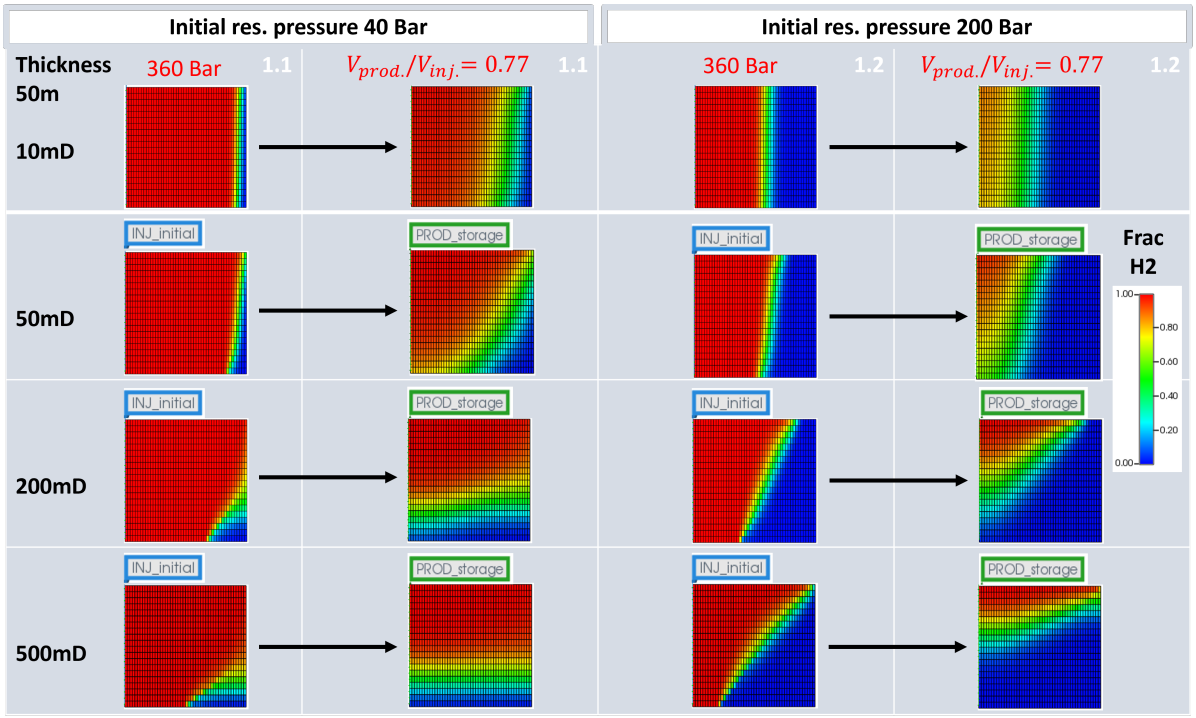

Figure 4.1: Visualization of one half of the cross-section of the performed radial reservoir experiment, with the injecting/producing well at the left hand side of the figures. The mole fraction of hydrogen is displayed at final moment of injection of hydrogen (before arrow) and at moment where the volume of recovered is 77.5% of that of the injected hydrogen (after arrow). Simulation 1.1 and 1.2 have an initial reservoir pressure of 40 and 200 bar (methane) respectively. More details on simulation parameters can be found in table 4.1 The figures are shown with a x:y ratio of 1:1, where the actual ratio should be 480:50. Therefore, the gravity effect is shown in a reduced way.

Figure 4.1 shows that increasing the permeability, at both higher and lower amounts of hydrogen in the reservoir, leads to an increased gravitational segregation effect. It is clearly visible that the bulk of hydrogen, depicted in red, is moving on top of the methane, depicted in blue. This effect is intensifying in the results of the simulations with higher reservoir permeability (lower rows).

4.2.2. VISUALIZATION RESULTS OF SIMULATION SETS 2.1 AND 2.2

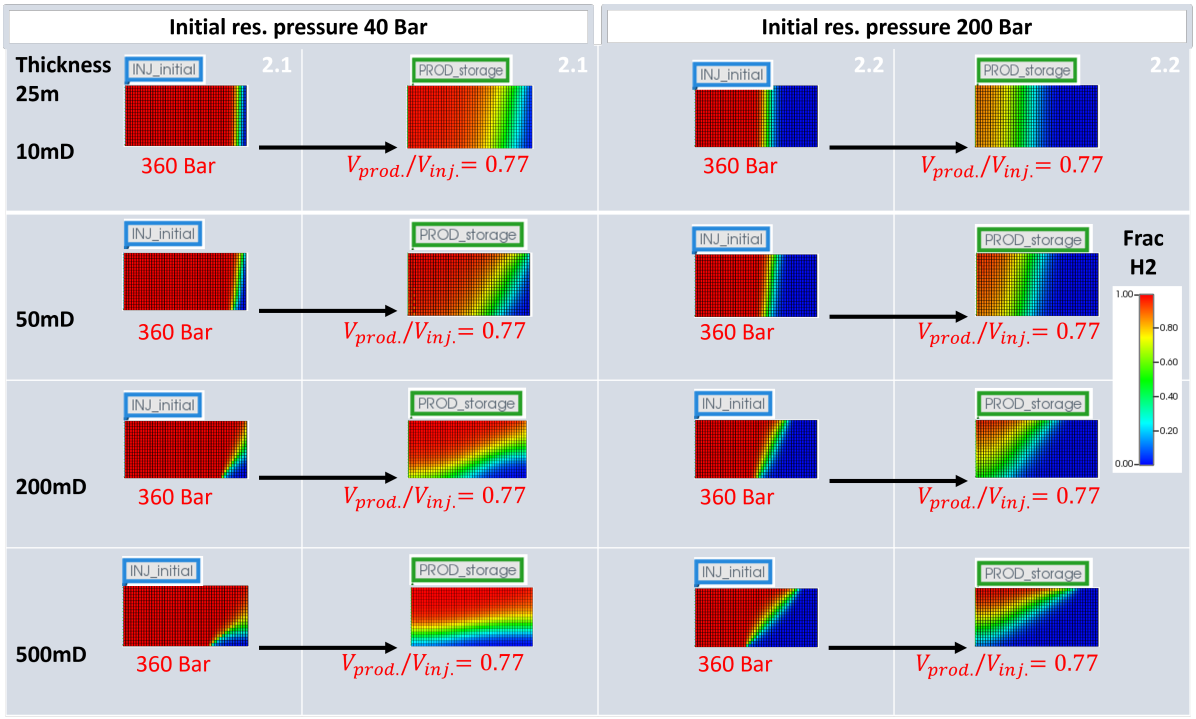

Figure 4.2: The same figure description as fig. 4.1 applies here. In these experiments however, the reservoir thickness is half of that of simulations 1.1 and 1.2. Therefore, the height of the visualization figures has been halved accordingly. The figures are shown with a x:y ratio of 2:1, where the actual ratio should be 480:25. Therefore, the gravity effect is shown in a reduced way.

Figure 4.2, where the same experiment is repeated a reservoir of half the thickness, also shows the effect of gravitational segregation. However, when comparing these results with those from fig. 4.1, it is evident that decreasing the reservoir thickness in this experimental setup, affects the distribution of the gases in the reservoir at the captured moment in time. The gravitational segregation has taken place to a lower extent in all the simulations of set 2.1 and 2.2 compared to set 1.1 and 1.2. The results of 2.1 and 2.2 are as if the lower section of 1.1 and 1.2 is cut off. This effect is clearly seen in the production cycle of the 200 mD runs of simulations 2.1 and 2.2 compared to the same runs in 1.1 and 1.2. In the concerning visualizations, it can be observed that pure methane (blue) has reached the production well through the bottom of the reservoir in 1.1 and 1.2, and it has not in 2.1 and 2.2. The observation described above automatically means that there is less methane breakthrough towards the wells at the left hand side of the figures, thus the production can continue longer without failing to meet the mole fraction production constraint set in section 4.1.1.

4.2.3. VISUALIZATION RESULTS OF SIMULATION SETS 3.1 AND 3.2

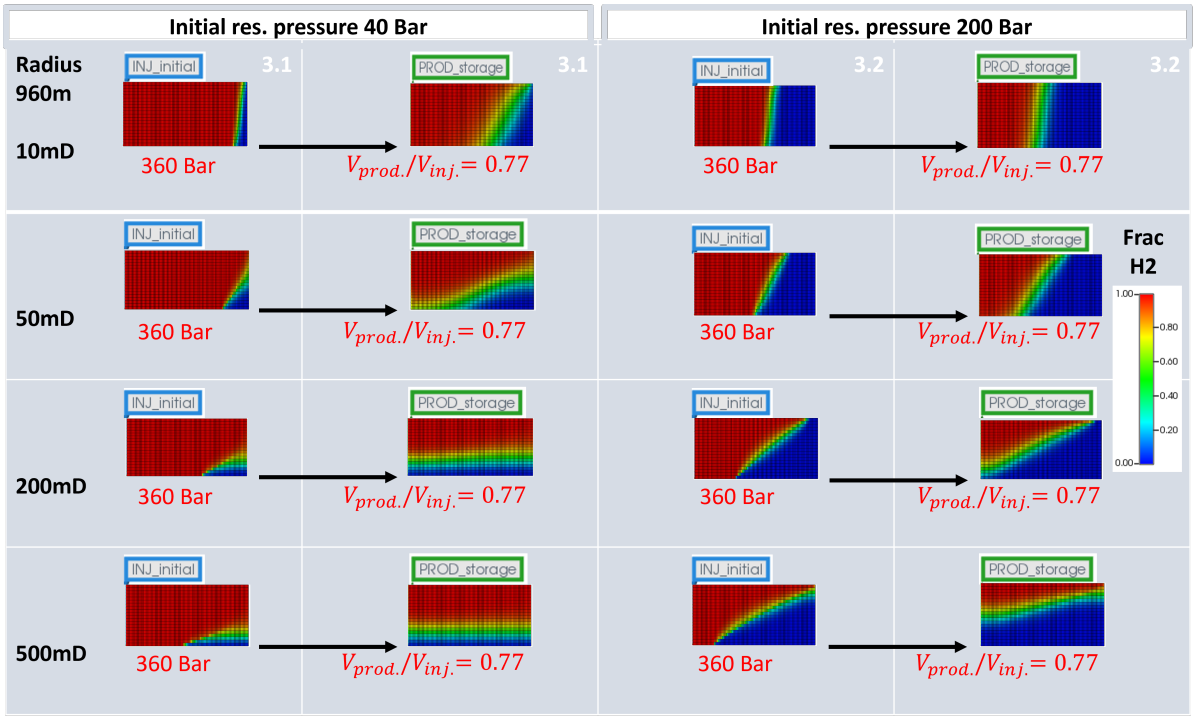

Figure 4.3: The same figure description as fig. 4.1 applies here. In these experiments however, the reservoir radius is double of that of simulations 1.1 and 1.2. The figures are shown with a x:y ratio of 1:1, where the actual ratio should be 480:50. Therefore, the gravity effect is shown in a reduced way.

In simulations 3.1 and 3.2, which are displayed in fig. 4.3, the experiment of 1.1 and 1.2 is repeated with double the reservoir radius. This means that the reservoir volume, which has a quadratic relation to the radius, is multiplied by four. This larger volume in combination with identical injection and production rates between the simulations, causes it to take a relatively long time to reach the final injection pressure of 360 bar. Due to this long simulation time, gravity has a stronger grip on the gases, causing a large gravitational segregation effect. This effect is evident from comparing the figures in fig. 4.3 to fig. 4.1, where the mixing front of the simulations in 3.1 and 3.2 are rotated more clockwise with respect to those in 1.1 and 1.2.

4.2.4. VISUALIZATION RESULTS OF SIMULATION SETS 4.1 AND 4.2

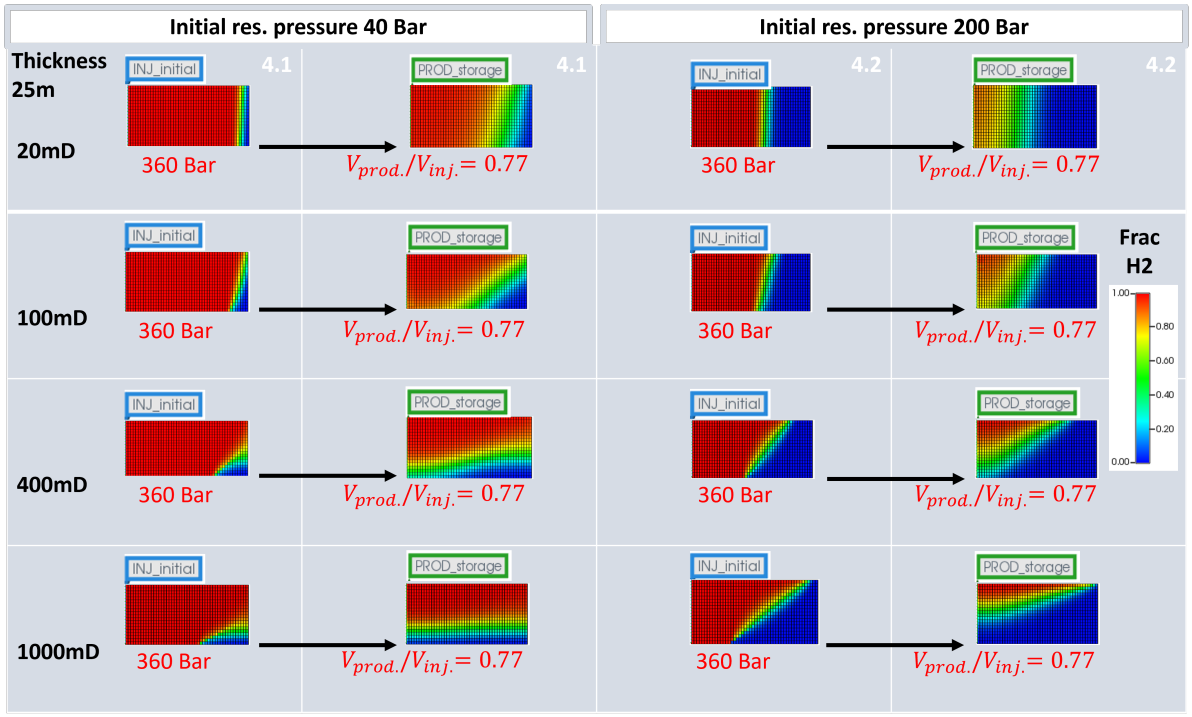

Figure 4.4: The same figure description as fig. 4.1 applies here. In these experiments however, the reservoir thickness and permeability are half and double that of simulations 1.1 and 1.2 respectively. This combination of thickness and permeability makes the thickness multiplied with permeability equal. The figures are shown with a x:y ratio of 1:1, where the actual ratio should be 480:50. Therefore, the gravity effect is shown in a reduced way.

In fig. 4.4 the results of simulations 4.1 and 4.2 are visualized, in which a combination of factors have their impact. Firstly, the reservoir thickness which is only half that of the reservoir in 1.1 and 1.2. This causes the reservoir volume to be only halve as much, making the injection time halve as long. Secondly the permeability values are double with respect of those in 1.1 and 1.2, making the the impact of gravity on the gases relatively large. Comparing the simulations of fig. 4.4 to those of fig. 4.1, the observed differences are minimal. It appears as if the product of thickness and permeability could be a critical factor in the positional behavior of these gases in the reservoir.

4.2.5. RESULT PLOTS OF THE EFFECT OF PERMEABILITY AND RESERVOIR DIMENSIONS ON THE RECOVERABLE VOLUME FRACTION OF HYDROGEN

In this section the plots corresponding to simulation sets from table 4.1 are presented. Figure 4.5a and fig. 4.5b show the volume fraction of hydrogen that is recovered without violating the rate and purity constraints set in section 4.1.1. This fraction is plotted as a function of permeability for three different reservoir dimensions and two different initial methane pressures as explained in table 4.1. From these plots it is evident that reservoir dimensions and permeability have a significant influence on the recoverability performance of the system. The first trend that can be observed in all plots is the negative relation between permeability and fraction of recovered hydrogen volume for all permeability values larger than roughly 100mD. This value might be slightly dependent on the reservoir dimensions, but is largely determined by the production rate constraint, which is explained in section 4.1.1. If the permeability decreases further than a critical value, the recovery rate will slow down fast enough to violate the rate constraint earlier than the mole fraction constraint, causing the recovered volume-fraction of hydrogen to decrease. These permeability values are represented by the circular shaped data points in the plot. On the other hand, increasing the permeability further than this critical number will decrease the recoverable volume-fraction of hydrogen too, as the impact of gravity on the position of the gases increases. From both plots it is evident that at the radial reservoir dimensions and conditions of simulation 1.1 and 1.2, decreasing the reservoir thickness is beneficial for the recoverable volume-fraction of hydrogen at higher permeability values. On the other hand, increasing the reservoir radius slightly decreases

the recoverable volume-fraction of hydrogen at high permeability values but increases it at the critical permeability value mentioned earlier. This increase in recoverable hydrogen around the critical permeability is more pronounced at the initial reservoir pressure of 200 bar methane than at 40 bar.

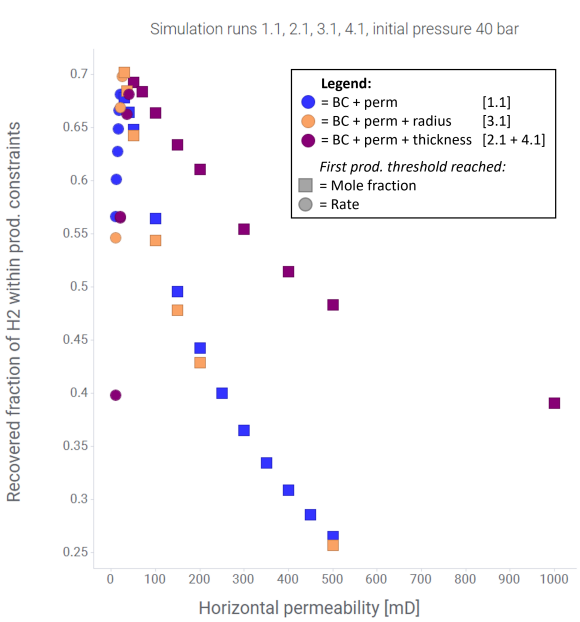

(a) Comparison of all simulations at initial pressure of 40 bar methane. The blue data points represent the base case where only permeability was varied. Yellow and purple represent the cases where besides permeability, the reservoir radius and thickness were varied respectively.

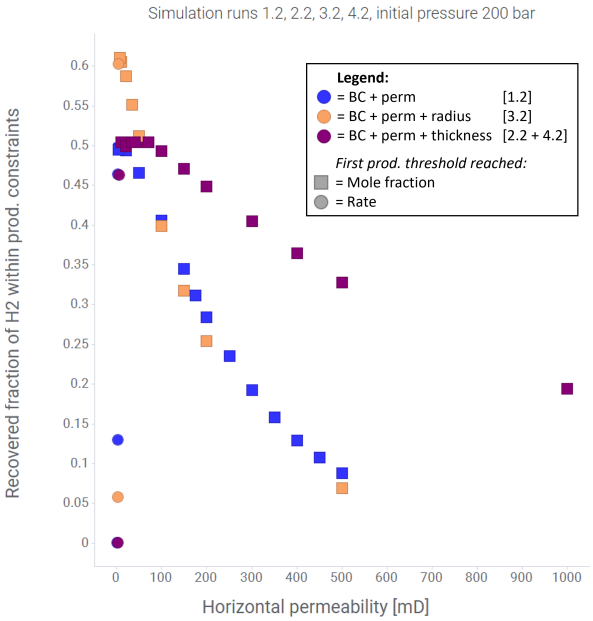

(b) Comparison of all simulations at initial pressure of 200 bar methane. The blue data points represent the base case where only permeability was varied. Yellow and purple represent the cases where besides permeability, the reservoir radius and thickness were varied respectively.

Figure 4.5: Plots showing recoverable volume fraction of hydrogen vs permeability for simulation sets from table 4.1

The plots in fig. 4.6a and fig. 4.6b show a comparison of the 40 and 200 bar initial methane pressure cases, where the fraction of recoverable hydrogen volume is plotted against permeability. Both in the base case of fig. 4.6a, where only permeability is varied and in the case where the reservoir thickness was halved, the the initial reservoir pressure of 40 bar has better hydrogen recovery results. This means that for these specific simulating conditions, the higher amount of hydrogen in the reservoir increases the fraction of hydrogen volume that can be recovered.

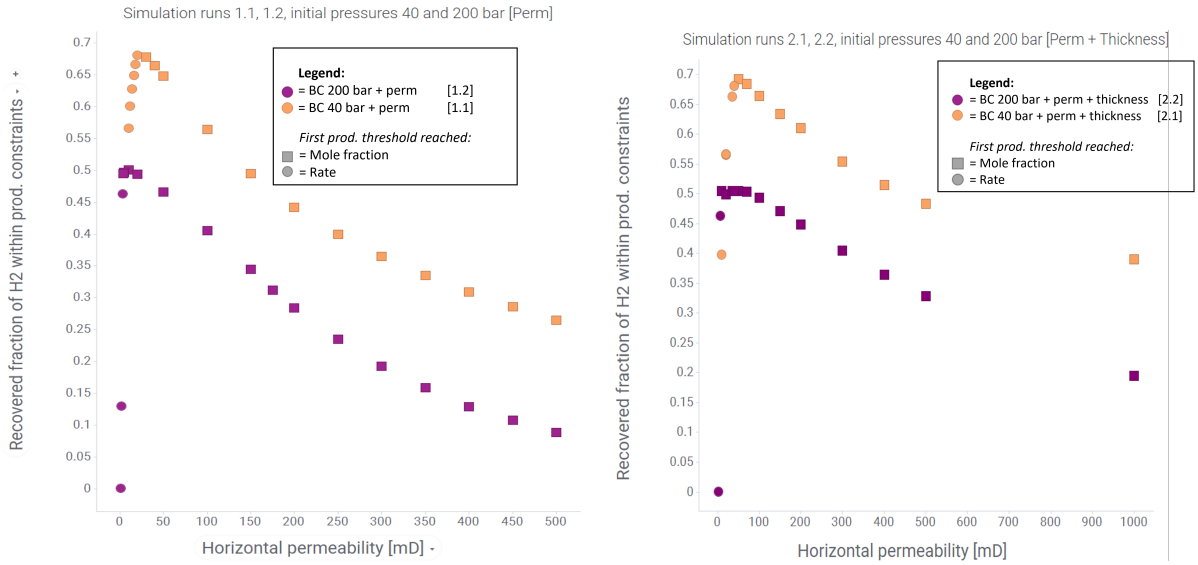

(a) Comparison of the base case simulations, where only the permeability is varied, for an initial methane reservoir pressure of 40 bar (yellow) and 200 bar (purple).

(b) Comparison of the 40 bar (yellow) and 200 bar (purple) initial methane pressure simulations where permeability and reservoir thickness are varied.

Figure 4.6: Plots showing recoverable volume fraction of hydrogen vs permeability. Comparison of different amounts of cushion gas.

5 | Physical & numerical dispersion

One of the main goals of modeling the flow and mixing of hydrogen gas stored in the subsurface, is to understand how the purity of the hydrogen gas can be maintained. In order to keep the hydrogen losses to a minimum, the mixing of hydrogen gas molecules with cushion gas molecules should be limited. From section 2.1 it is clear that diffusion and dispersion are factors that influence the development of the mixing front through the reservoir. However, they are not the only factors influencing the modeling results related to the mixing zone. Numerical dispersion is another dominant factor in simulating miscible displacement of fluids [23]. The effect of numerical dispersion on the mixing zone can be analyzed by simulating hydrogen gas injection into a methane filled reservoir while excluding the processes of mechanical dispersion and effective molecular diffusion. This way, eq. (3.1.2) is executed without a contribution of its dispersivity term. The numerical dispersion is a result of the transmissibility term [41] in eq. (3.1.2), which is in turn dependent on the distance between two grid points 3.1.3. [23] Therefore, a change in grid cell size will influence the contribution of numerical dispersion to the mixing zone, enabling the comparison of physical- and numerical dispersive mixing.

5.1. Objectives and methodology

The goal of the simulations in this chapter is to increase the understanding of the (numerical) dispersive processes and their impact on the mixing zone between hydrogen and Methane gas in the reservoir. Furthermore the possibility to substitute physical dispersion with numerical dispersion is explored by varying the grid cell' and time step sizes. The GEM simulator is capable of simulating the dispersive and diffusive physical processes described in section 2.1. The keywords *DIFFC-GAS and *DISPERARRAY-LNG are set in the GEM input, activating the diffusion and dispersion respectively. *DIFFC-GAS defines the diffusion rate in the gas phase and should be entered in cm^2/s. *DISPERARRAY-LNG defines the scale dependent longitudinal dispersivity value, which should be entered in meters. The total dispersive flux is calculated by GEM through eq. (5.1.1), where $D_{t,ik}$ is the physical dispersion, which was earlier explained in eq. (2.3.1).

$$J_i = -\sum_k \phi \rho_k S_k D_{t,ik} \nabla yik \tag{5.1.1}$$

*DIFFC-GAS represents the $D_0\phi^m$ term of eq. (2.3.1) and *DISPERRAY-LNG defines the α term, which is scale dependent as described in section 2.4.

5.1.1. Experimental configuration

The experiments are conducted on the base case reservoir model of section 3.3, which is initially filled with 100% CH_4 at 200 Bar. Consequently, pure hydrogen is injected for at 5E+6 Nm^3/day for 52 consecutive days. After 52 days, the width of the mixing zone is analyzed. This process is repeated in six simulation experiments, each with multiple runs, according to table 5.1. During the experiments specific parameters are varied in order to test their influence on the mixing. The experimental setup is shown in fig. 5.1.

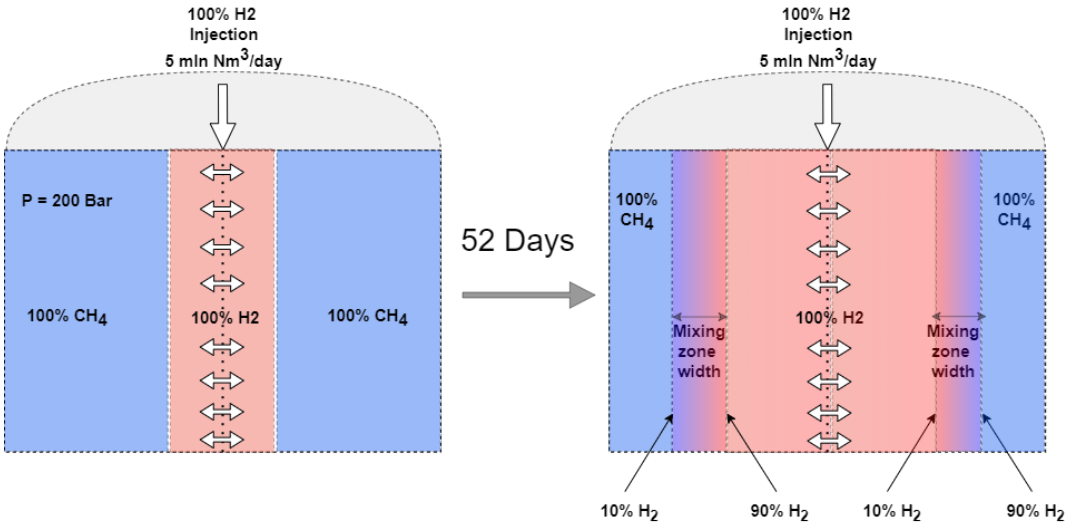

Figure 5.1: conceptual visualization of the simulation experiment in chapter 5. Mixing zone width is illustrated, which is distance between 10% and 90% mole fraction H_2 in the reservoir.

5.2. EXPERIMENT DESCRIPTION

Six simulation experiments are discussed in this chapter, which are listed and explained in more detail below. Each of the experiments consists of a number of simulation runs. See table 5.1 for an overview of the simulation experiments and corresponding parameters that are analyzed.

1. experiment number 1, the higher order TVD option in GEM, which was explained in section 2.9, is tested on a range of cell sizes from 0.15m up to 48m. The goal is to quantify its effect on the mixing zone width.

2. In experiment number 2, the range of time steps and cell sizes is determined, for which computational time is adequately low on a standard office laptop (within a few hours), and numerical dispersion is nearly absent. The range of cell sizes tested is from 0.15m up to 1m length. This range is chosen because earlier simulations showed no potential for excluding numerical dispersion at larger cell sizes. The range of time steps tested is from 0.1s up to 0.5s. This experiment should lead to a a suitable cell size and time step at which the effect of physical dispersion can be analyzed in experiment 3.

3. In experiment number 3, the process of hydrogen injection is repeated in multiple simulations with dispersivity values ranging from 0.1m up to 4m. No effective molecular diffusion is set in the simulations of experiment 3. The cell size in radial direction is 0.15 and the time step is 0.01s, which were obtained from experiment 2. This time resolution was found to practically exclude all numerical dispersion. This way, purely the influence of mechanical dispersion on the development of the mixing zone is analyzed.

4. In experiment number 4, the process of hydrogen injection is repeated in multiple simulations with different effective molecular diffusion. The dispersivity value is 1m in all simulations of experiment 4. The cell size in radial direction and time step during these simulations are 0.15m and 0.01s respectively and were obtained from experiment 2. This resolution scale was found to practically exclude all numerical dispersion. This way, purely the influence of effective molecular diffusion on the development of the mixing zone is analyzed.

5. In experiment number 5, the process of hydrogen injection is repeated in multiple simulations with different radial cell sizes (i-direction). No dispersivity and diffusion coefficient are set in these simulations. This way, purely the influence of numerical dispersion on the mixing zone is isolated. As explained in section 2.8, the numerical dispersion is expected to increase with cell size.

6. Experiment number 6 is similar to experiment 5, in a way that multiple simulation runs are done with different cell sizes. However, during the simulations in this experiment, dispersivity and diffusion are set to 1m and 4.46E-5 cm^2/s respectively to analyze the combined effect of physical and numerical dispersion on the mixing zone.

For each of the simulation runs in the experiments, the mixing zone width is analyzed after 52 days. Thus, the injected volume (Nm^3) of hydrogen is equal in all of the runs because of the identical injection rates. The simulation parameters of the experiments in this chapter are displayed in table 5.1. The permeability is 20mD for all simulations in order not to let gravity have a significant effect on the gases, which could disturb the analysis of the mixing zone. Moreover, the height of the reservoir is represented by a single cell in k-direction in order to decrease simulation time. The thickness of this single layer is 50 meters, making the total height and volume of the reservoir equal to the reservoir in section 3.3.

Table 5.1: Simulation parameters for experiments 1,2, and 3

Parameters	**BC Value**	**Exp. 1**	**Exp. 2**	**Exp. 3**	**Exp. 4**	**Exp. 5**	**Exp. 6**	**Unit**
Initial res. gas	CH_4							[-]
Injected gas	H_2							[-]
Initial res. press.	200							[bar]
Inj. target	52							[day]
Max. inj. rate	5E+6							[Nm^3/day]
Inj. well location	Center							[-]
Time step	0.01 - 0.2		0.1 - 0.05	0.01	0.01			[day]
Cell size	0.15 - 48		0.15 - 1.0	0.15	0.15			[m]
Res. thickness	50							[m]
Res. radius	480							[m]
Res. temperature	90							[$^\circ C$]
Permeability	20							[mD]
k_z/k_i	0.1							[-]
Porosity	0.12							[-]
Saturation	0.15							[-]
Dispersivity	0			0.1 - 4.0	1.0		1.0	[m]
Diffusion coeff.	4.46	0	0	4.46	3.4 - 4460	0		[$*10^{-5}$ cm^2/s]
Num. disp. control	On	On & off						[-]

5.3. RESULTS

In this section, the results of the experiments described in section 5.2 are presented. Experiment 2 and 3 are displayed below in section 5.3.1. Experiment 2 serves as exploration for a suitable resolution for experiment 3.

5.3.1. EXPERIMENT 2 AND 3

fig. 5.2a shows that both time step size and cell size in i-direction significantly affect the mixing zone, indicating significant numerical dispersion. From the three data points representing a cell size of 1m, it can be seen that decreasing the time step from 0.05s to 0.01s has a relatively large effect on the mixing zone width, which decreases from 10m to 5m. Decreasing the time step further, by a factor 10 , from 0.01s to 0.001s, results in a relatively insignificant mixing zone width reduction from 5m to 4.5m. The simulation running time however, increases by a factor 8 between the mentioned data points. Decreasing the time step size at smaller cell sizes has a similar effect. Decreasing the cell size from 1m to 0.15, while maintaining the same a constant time step, only results in a relatively insignificant mixing zone width reduction from 5m to 4m, while the simulation running time increases from 8min to 53min ≈ factor 7.

In experiment 3, of which the results are displayed in fig. 5.2b, the goal is to simulate with an adequately small grid cell size and time step to diminish numerical dispersion, and consequently test the effect of different dispersivity values on the mixing zone width, as shown in fig. 5.2a. for this reason, the cell size in i-direction and time step size were set to 0.15m and 0.01 for all simulations in experiment 3. The mentioned resolution results in a mixing zone width of roughly 4m (numerical dispersion) when no physical dispersion is included in the simulation. The figure shows that an increase in dispersivity up to 4m, which was stated as reliable in section 2.4, results in a significant increase in the mixing zone width. The base value of 1m dispersivity causes the mixing zone width to increase to 30m. The effective molecular diffusion of 4.46E-5 cm^2/s, which was calculated through eq. (2.5.6) and eq. (2.3.1), is set in all simulations corresponding to the red data points. The blue data point represents a simulation without diffusion. However, comparing the results of the red

and blue data points at a dispersivity of 0, it becomes clear that the effect of the mentioned diffusion value is insignificant, as the mixing zone only increases from 4m to 4.3m. It can be seen from fig. 5.2b that any inclusion of the dispersivity values in the given range has a far larger effect than the mentioned diffusion.

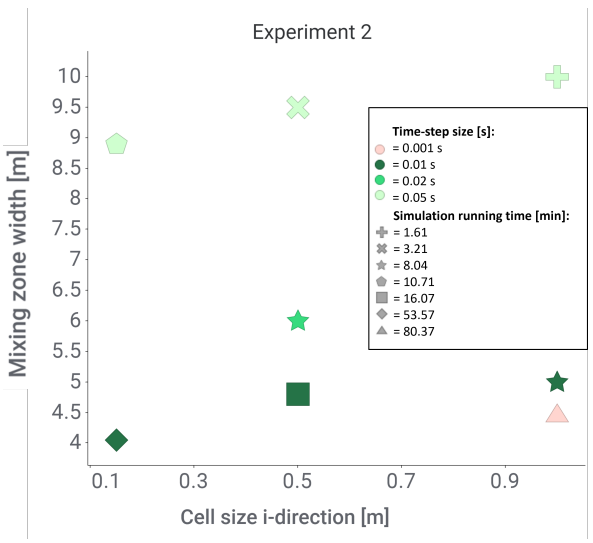

(a) Experiment 2, in which the effect of cell size (x-axis) and time step size (color) on the mixing zone width are analyzed. The simulation running time of each data point is displayed as its shape.

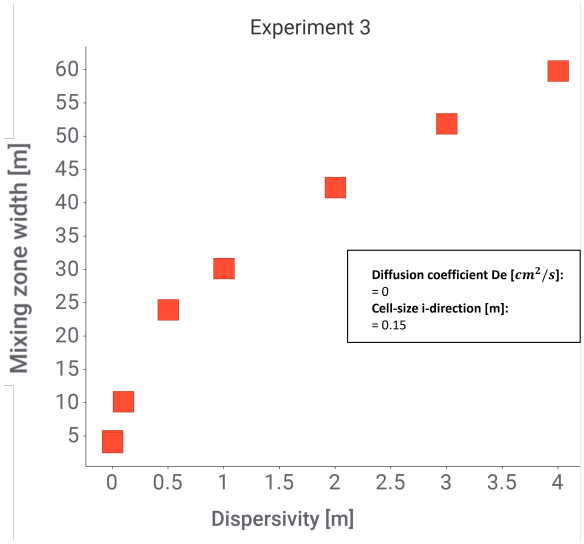

(b) Experiment 3, in which the effect of the mechanical dispersion on the mixing zone width is analyzed. The Diffusion coefficient D_e is set to 4.46E5 and 0 cm^2/s for the simulations represented by the red and blue data points respectively.

Figure 5.2

5.3.2. EXPERIMENT 1 AND 4

All of the data points represent simulations where the mechanical dispersion is activated by setting the dispersivity to the base case of 1m. Each of the data points represents a different effective molecular diffusion. The left three data points of fig. 5.3a represent three simulations with effective molecular diffusion values around 4.46E-5 cm^2/s, which are realistic for H_2-CH_4 at reservoir conditions, as calculated by eq. (2.5.6). However, these three data points, show no visible change in mixing zone width (30m) compared to the result of a simulation with only mechanical dispersion included. Therefore, the effective molecular diffusion is increased three orders of magnitude to see at which values the effective molecular diffusion starts to have a significant effect on the mixing zone width compared to mechanical dispersion. At an increase of one order of magnitude, at 4.0 E-4 cm^2/s there is no visible effect on the mixing zone. At an increase of two orders of magnitude with respect to the realistic values, the mixing zone increases from 30m (mechanical dispersion only) to 32m. At an increase of three orders of magnitude to 4.0 E-2 cm^2/s, the effective molecular diffusion has started to compete with the mechanical dispersion by increasing the mixing zone width to 45m.

In experiment 1,the effect of numerical dispersion on the mixing zone is tested in combination with and without numerical dispersion control 2.9. Numerical dispersion is included by increasing the cell size and time step size in the simulations, without having any physical dispersion set in the simulator. This is represented by the blue data points without dispersion control, where a significant increase in the mixing zone width is witnessed towards the larger cell sizes. The numerical dispersion control option (red data points) is effective in reducing the numerical dispersion, as the mixing zone reduces by a substantial amount. For a cell size of 30m, the mixing zone width reduces from roughly 120m to 65m. From the set of data points it can be seen that the effectiveness of the numerical dispersion control is largest at smaller cell sizes. It seems like the reduction of the mixing zone upon activating the numerical dispersion control doesn't increase at cell sizes over 20m. Therefore, the fraction of the mixing zone that is reduced upon activating numerical dispersion control is larger at lower cell sizes. For example, the mixing zone decreases from 50m to 20m at a cell size of 5m, and it reduces from 120m to 65m at a cell size of 30m. The latter of which is a relatively smaller reduction.

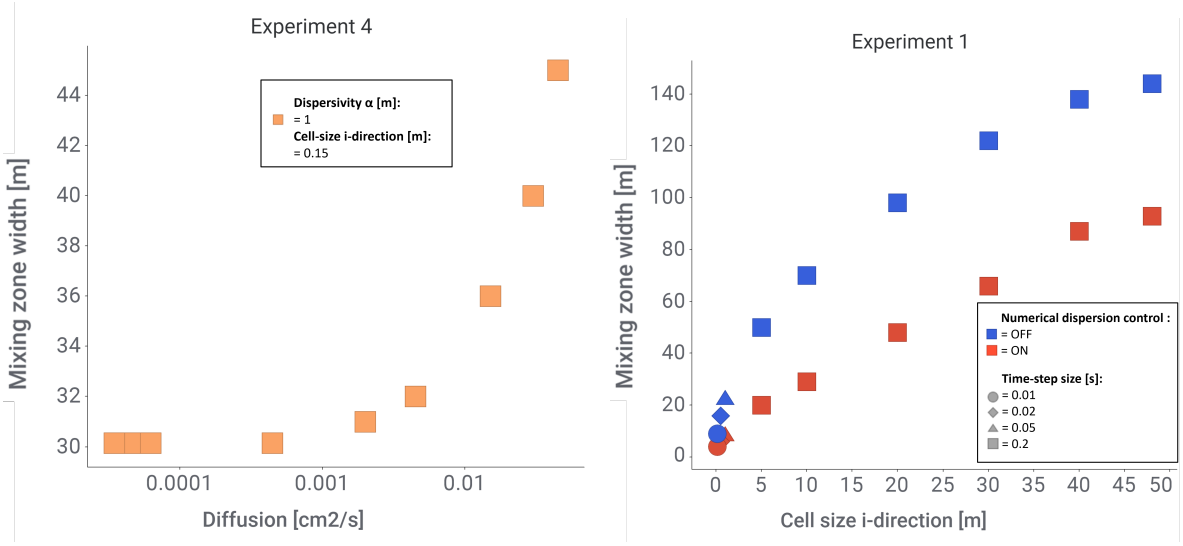

(a) Experiment 4, in which the effect of the effective molecular diffusion on the mixing zone width is analyzed compared to mechanical dispersion. The dispersivity is set to 1m for all simulations in the experiment.

(b) Experiment 1, in which the effect of the numerical dispersion control option in GEM is on the mixing zone width is tested. The red and blue data points represent the simulations with and without dispersion control respectively, in which the cell size and therefore the numerical dispersion is increased.

Figure 5.3

5.3.3. CONCEPTUAL VERIFICATION OF EXPERIMENT 4

The results of the numerical simulation in experiment 4 shown in fig. 5.3a, indicate that the influence of effective molecular diffusion at the simulated reservoir conditions is negligible compared to mechanical dispersion. The effective molecular diffusion calculated for these conditions should be increased by two orders of magnitude in order to increase the mixing zone from 30 meters caused only by mechanical dispersion , to 32 meters caused by both mechanical dispersion and effective molecular diffusion. In order to verify these results, the contribution of mechanical dispersion and effective molecular diffusion to the physical dispersion are conceptually calculated in this section. For these calculations the value 1.0 is be entered for dispersivity, as in experiment 3. The effective molecular diffusion ranges from 4.65E-9 m^2/s to 4.65E-6 m^2/s, as in experiment 3, where the the realistic value for diffusion between H_2-CH_4 molecules at reservoir conditions is calculated through eq. (2.5.6) and eq. (2.3.1). The results of the conceptual calculations are depicted in fig. 5.4.

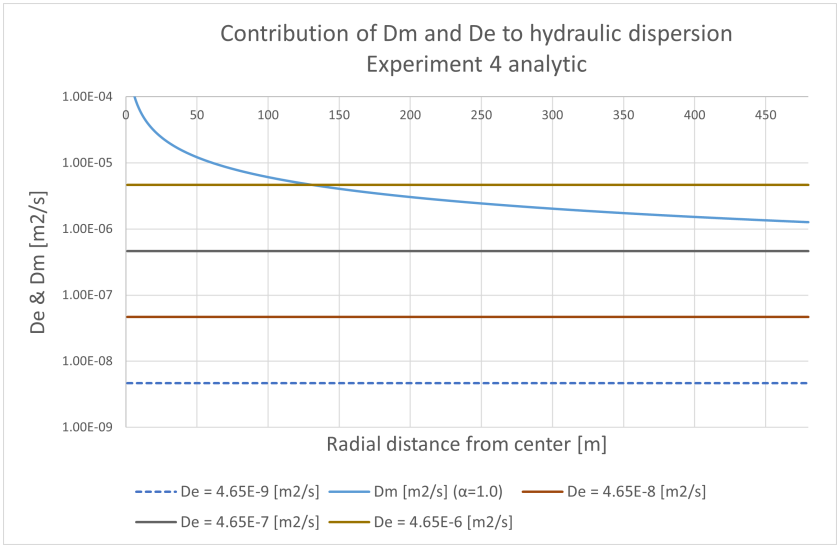

Figure 5.4: conceptual calculation of the contributions of the mechanical dispersion (D_m) and effective molecular diffusion (D_e) to the physical dispersion. The value of D_e is ranged over 4 orders of magnitude to compare its contribution to a dispersivity of 1m

From fig. 5.4 it is evident that the effective molecular diffusion coefficient of 4.65E-9 m^2/s, which is the calculated value for at the examined reservoir conditions, is negligible to the mechanical dispersion coefficient. The same is true if the effective molecular diffusion is raised by one or two orders of magnitude, although raising it by two orders of magnitude to 4.65E-7 m^2/s brings the effective molecular diffusion to roughly one fifth of the mechanical dispersion coefficient at a radial distance 280m from the center of the reservoir, which is the distance at which the mixing zone is located after 55 days of injection. Only after raising the effective molecular diffusion by three orders of magnitude to 4.65E-6 m^2/s, it is contributing a roughly equal amount to the physical dispersion as the mechanical dispersion does. The results of these conceptual calculations are in line with the results of the numerical simulations shown in fig. 5.3a. For inclusion of the full range of dispersivity 0.1-4.0 in the comparison, see

5.3.4. EXPERIMENT 3, 5 AND 6

fig. 5.5a compares the mixing zone width of the simulations with solely numerical dispersion (yellow data points) with that of the simulations with a dispersivity of 1m (purple data points). It can be noted from the figure that the yellow and purple data points are positioned closer to one-another upon increasing the cell size. This means that the effect of physical dispersion is significant when numerical dispersion is absent but reduces towards zero once numerical dispersion increases.

in order to see at what cell sizes the effect of numerical dispersion on the mixing zone is equal to the effect of physical dispersion, experiment 3 and 5 are displayed together in fig. 5.5b. As displayed by the red-dotted lines, the effect of the various purple data points (physical dispersion) on the width of the mixing zone, is equal to that of the yellow data points (numerical dispersion) which are on the same level on the y-axis.

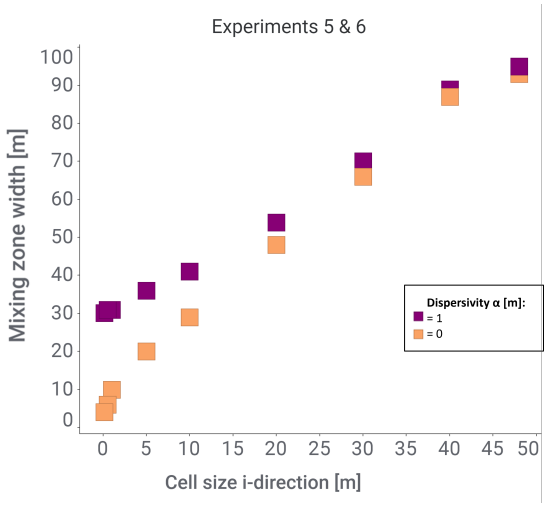

(a) The mixing zone width is analyzed as a function of cell size, where dispersivity is set to 0 (yellow) and 1 (purple) in order to compare the effects of numerical- and physical dispersion on the mixing zone.

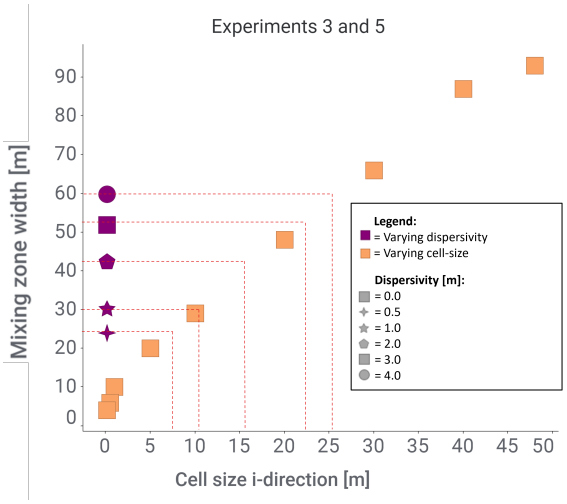

(b) The purple data points (experiment 3) represent simulations with different dispersivity values, indicated by their shape, without influence of numerical dispersion. The yellow data points (experiment 5) represent simulations with different cell size (numerical dispersion) without any physical dispersion.

Figure 5.5

5.3.5. CONCEPTUAL VERIFICATION OF EXPERIMENT 3

In order to verify that the obtained simulation results regarding the effect of physical dispersion on the width of the mixing zone are in line with the expected physical behavior, conceptual calculations are done for the setup of experiment 3. The calculations are consistent with the explained theory from section 2.5.1, which is valid for homogeneous one-dimensional porous media. The physical dispersion is calculated through eq. (2.3.1), for which the flow velocity of 2.17E-6 m/s after 55 days is calculated by multiplying the cumulative injection time by the injection rate of 5E6 Nm^3/day and evaluating the injected volume for the radial reservoir with dimensions as shown in table 3.1. The Peclet number is calculated through eq. (2.5.3), for a reservoir length of 480m and a porosity of 0.12. The mixing zone width is calculated through eq. (2.5.5), in which the dimensionless time is taken 0.75 because the analyzed situation is after 52 out of 70 days of total injection. The mixing zone width is calculated for the simulated dispersivity values, ranging from 0 to 4m.

The results are displayed in section 5.3.5 and fig. 5.6. From comparing the mixing zone in section 5.3.5 with the corresponding dispersivity values in fig. 5.5b, it is evident that the 1D conceptual calculated values of the mixing zone are close to the simulated values. However, for each dispersivity value, the simulated case shows a mixing zone width which is roughly 20% higher than the conceptual case. This difference agrees well with the findings on numerical dispersion from fig. 5.2a, showing that a mixing zone is present even for a small grid cell size of 0.15m when no physical dispersion is included in the simulation. This contribution of numerical dispersion to the mixing zone, which proves to be inevitable at practically feasible cell sizes during the simulations, causes the simulated values to be higher than the conceptually calculated values.

Dispersivity [m]	$D_m[m^2s^{-1}]$	$D_e[m^2s^{-1}]$	Peclet number	Mixing zone [m]
0	1.09E-05	4.65E-09	1.87E+06	1.1
0.1	2.22E-07	4.65E-09	3.92E+04	7.6
0.5	1.09E-06	4.65E-09	7.97E+03	16.9
1.0	2.18E-06	4.65E-09	3.99E+03	23.9
2.0	4.35E-06	4.65E-09	2.00E+03	33.7
3.0	6.52E-06	4.65E-09	1.33E+03	41.3
4.0	8.69E-06	4.65E-09	9.99E+02	47.7

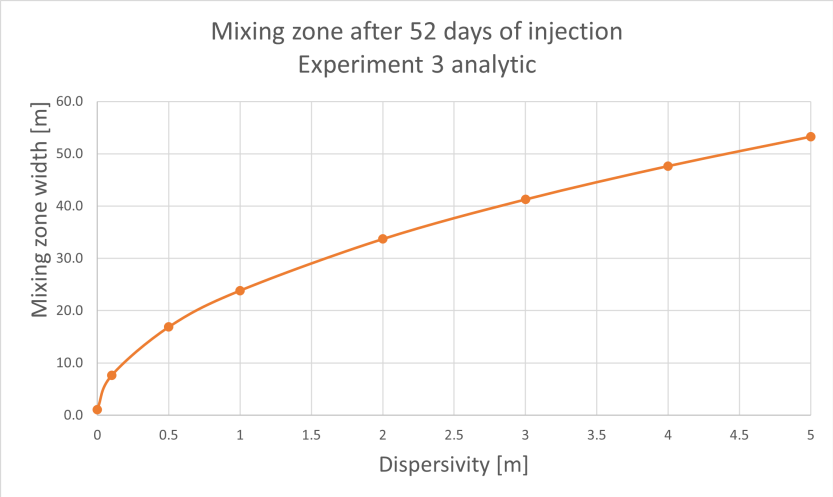

Figure 5.6: Conceptual calculation of mixing zone width for range of dispersivity values from exp_3

6 | Conclusion, Discussion & Recommendations

6.1. Conclusion

The results presented in this thesis indicate the importance of mixing processes during UHS in gas reservoirs. The mixing of hydrogen and cushion gas caused by gravity override and mechanical dispersion cannot be overlooked. Relatively small changes in permeability, reservoir dimensions and dispersivity can lead to significant changes in the amount of mixing. This will result in an earlier or later breakthrough of cushion gas and therefore changes the fraction of stored hydrogen that can be recovered under the assumed purity constraints. The compositional reservoir simulator CMG GEM has been used to capture the mixing processes for UHS in gas reservoirs. One of the main challenges of numerically simulating physical processes is being able to make a distinction between the effects of numerical dispersion and modeled physical phenomena. This subject is strongly related to the main research question, as introduced in section 1.3.1:

- How can the mixing processes related to underground hydrogen storage in gas reservoirs be simulated in a realistic way?

In order to introduce an answer to the main research question, the sub research questions below are answered first. In the the first three sub questions, the contributions of the three physical mixing processes related to UHS are investigated, as well as their implementation in a reservoir simulator.

- What is the significance of gravity override for UHS in gas reservoirs, and how can this mixing process realistically be captured in a reservoir simulator?

  This mixing process is a result of density difference between multiple gases in the reservoir, causing the lighter component to move upward. Gravity override is relatively easy to include in a compositional reservoir simulator because the material balance equation for fluid flow takes into account density differences between the components, which are calculated by the equation of state. The results of the simulations on gravity override indicate an increase in the gravity override as the permeability of the reservoir increases. There is a trade off concerning the reservoir permeablity. A higher permeability reservoir will lead to higher flow rates of the produced and injected gas. However, it also results in an earlier breakthrough of cushion gas with the produced hydrogen due to gravity override. A lower permeability reservoir will lead to lower flow rates of the produced and injected gas. However, it also results in a later breakthrough of cushion gas with the produced hydrogen. Furthermore, the degree of gravitational segregation is dependent on the reservoir thickness. The results of section 4.2 indicated that for a reservoir having half the thickness, a higher mole fraction of hydrogen remained at the lower section of the reservoir after the same injection/production scheme was used. Upon doubling the permeability values for the experiments with halved reservoir thickness, the gravitational segregation was restored to similar levels of the original simulation experiments, suggesting that the product of permeability and thickness is a decisive factor for gravitational segregation.

- What is the significance of mechanical dispersion for UHS in gas reservoirs, and how can this mixing process realistically be captured in a reservoir simulator?

  Mechanical dispersion is a porous medium dependent mixing process caused by microscale flow behavior and scales with fluid velocity, and is described by the left term in eq. (2.3.1). The microscale fluid flow variations determining dispersivity are caused by non-uniform velocity profiles along the cross section of individual pores, by distribution of pore sizes, or by the tortuosity of flow paths. Mechanical dispersion is optional in the compositional reservoir simulator used for this study and uses the scale dependent dispersivity as an input. The simulator includes the dispersive flux into the material balance for fluid flow, where it causes mixing between the different components. The simulator should run fully implicitly if physical dispersion is incorporated. Dispersivity is a parameter that has been the topic of discussion in the relevant literature, as mentioned in section 2.4. There is much uncertainty about the value range of this parameter and the degree of its dependency on reservoir length

scale. The authors mention that large scale and long term field experiments have to be conducted to gain more knowledge on this length scale dependency of dispersivity. Furthermore, even if the most realistic dispersivity value was known for each reservoir, the effect of mechanical dispersion on mixing is influenced by numerical dispersion in reservoir simulations. Therefore, as long as there is any numerical dispersion involved in a simulation, the simulated effects of mechanical dispersion might be overshadowed, and the overall effect of dispersion might be overestimated. If the cell size in a hydrogen injection simulation is increased at a constant dispersivity value, the mixing zone will be wider as a result of numerical dispersion, and therefore the mixing front is located further away from the injection well. This causes the flow velocity and therefore the mechanical dispersion at the front to be lower. For the reasons mentioned above, it seems unlikely that mechanical dispersion has yet been captured in a realistic way in a reservoir simulator.

- What is the significance of effective molecular diffusion for UHS in gas reservoirs, and how can this mixing process realistically be captured in a reservoir simulator?

  The effective molecular diffusion can be set as input in the compositional reservoir simulator, which adds to the dispersive flux and therefore the material balance for fluid flow. Because of the relatively high flow velocities at the investigated reservoir scale, effective molecular diffusion had a low contribution to the mixing compared to mechanical dispersion in the investigation performed here.

The significance of the three physical mixing processes and their behavior in UHS simulations is discussed in the answer to the first three sub questions. The last two sub questions are related to numerical dispersion, which intrinsically results from using a reservoir simulator. It should be noted that physical dispersion consists of mechanical dispersion and effective molecular diffusion.

- How does numerical dispersion quantitatively relate to physical dispersion in UHS simulations?

  The base case model has a radial cell size of 10 m, which is small by reservoir engineering standards [18]. At this cell size numerical dispersion causes a large mixing zone, especially when compared to a mixing zone that one would expect to be caused by mechanical dispersion at a dispersivity of 1 m. By using a higher order scheme for numerical dispersion control, numerical dispersion causes a much smaller mixing zone, similar to a mixing zone that one would expect to be caused by mechanical dispersion at a dispersivity of 1 m. By strongly decreasing the cell size and timestep to values of 0.15 m and 0.01 s respectively, the numerical dispersion can be reduced to such levels that it has a small contribution to the mixing zone compared to the analytically calculated mechanical dispersion. However, this reduction in cell size and timestep increases computational time significantly.

- How can physical dispersion realistically be simulated, taking into account the existence of numerical dispersion?

  There are essentially two possible options to simulate physical dispersion in a way that could approximate reality. One is to substitute physical dispersion with numerical dispersion by simulating at a specific cell size for which the mixing zones are of similar magnitudes. In this thesis, this has only been tested for single cycle UHS simulations. The other option is to try and minimize numerical dispersion by using a combination of a higher order scheme and decreasing the cell size and time step enough to suppress numerical dispersion to acceptable levels.

With the five sub questions discussed, the main research question is revisited below.

- How can the mixing processes related to underground hydrogen storage in gas reservoirs be simulated in a realistic way?

  In order to capture the mixing processes related to UHS in a reservoir model, the three related mixing processes have to be incorporated. The process of gravitational override is simulated by the compositional simulator by calculating densities of the different gas components during hydrogen injection and production. Effective molecular diffusion is simulated in CMG GEM by including it in the transport equation. If mechanical dispersion is to be simulated, a realistic value for dispersivity is needed. However, a lot of uncertainty exists in the literature regarding the correct value of this parameter, which represents the flow variations at micro scale. After reviewing the literature, it was decided to use the values of 0.5 m up to 4.0 m. These are the lower and upper bound values found from experimental

sandstone dispersivity data that was classified as most reliable by Gelhar *et al.* 1992 [4]. Modeling the three mentioned physical mixing processes is automatically accompanied by numerical dispersion, which is intrinsically incorporated in a reservoir simulator. Numerical dispersion should either be reduced to an acceptable level or be used as a substitution for physical dispersion in order to approach the reality as best as possible.

6.2. DISCUSSION

6.2.1. IMPLICATION OF THE RESULTS

This section describes the alignment of the results with existing research related to UHS in gas reservoirs. Previous statements about diffusion from Feldmann *et al.* 2016 [18] state that the effective molecular diffusion is considered as a slow process when compared to advective/convective transport and mechanical dispersion. This has been confirmed for the modeled radial reservoir with specific dimensions in this thesis.

The results in this thesis differ from the work of Feldmann *et al.* 2016 [18] in terms of gravity override. They mention that gravity override plays a minor role in UHS in gas saturated reservoirs. The work in this thesis has shown the relevance of gravity override, with permeability and reservoir thickness as its main controlling factors. The difference between the mentioned study and this thesis could be caused by the fact that Feldmann *et al.* 2016 [18] have analyzed the gravity effect on reservoirs with more realistic, heterogeneous permeability and high permeability streaks, resulting in a more pronounced advection compared to gravitational effects.

A general assumption in underground gas storage is that during underground natural gas storage, injection of natural gas into a storage reservoir moves the indigenous gas in a piston-like movement, with very little mixing of the molecules of injected and indigenous gas [25]. It is shown in this thesis that all considered physical dispersion values result in significant mixing of hydrogen with the indigenous cushion gas. Therefore, the results of this thesis provide new insight into the relationship between mixing in UHS and UGS operations. Note that this is far more important for UHS than for UGS, since for UGS the injected gas does not differ (so much) from the resident gas compared to the situation of UHS.

Most of all, this thesis contributes to a solid foundation for further simulation work on UHS in gas reservoirs. Earlier work on this subject has not focused on either the wide range of the dispersivity values found in the literature, or the magnitude of numerical dispersion in the (mixing) results of numerical simulations. Creating a solid foundation on the mentioned topics is critical for continuation with more complex multicycle (injection-production) simulations and sensitivity analysis.

6.2.2. LIMITATIONS

Despite the fact that this thesis can provide a solid foundation in the field of UHS simulations, it has some limitations, which are elaborated in this section. Starting with the limitations resulting from the way the physical concepts are adopted, and followed by the limitations of the used reservoir model.

It is beyond the scope of this study to address the question of biochemical degradation and dissolution of hydrogen, which is the subject of focus for a variety of other research such as Amid *et al.* 2016 citeAmid2016SeasonalReservoir and Pichler 2013 [44]. These conclude that up to 3.7 % and 1.0 % of the stored hydrogen volume could be lost due to bacterial conversion and reactivity with reservoir rock respectively within the cyclic period of 80 days. Furthermore, they concluded that up to 0.1 % of the stored hydrogen volume could be lost due to dissolution and diffusion into the reservoir rock and aquifer water over a storage period of 120 days. Variations in intensity of biochemical degradation of hydrogen might result in lower hydrogen mole fractions over multiple cycles.

The reservoir model that was built and used for this thesis is a radial model with a radius of 480 m and a thickness of 50 m. Modelling a reservoir of this type and size gives a tolerance for decreasing grid size and time step size without extremely increasing the computational time. However, converting a 480 m radial model to a Cartesian or corner point grid model increases the amount of grid cells significantly. This will undoubtedly have a large effect on the computational time, especially if reservoirs of larger dimensions are considered, which are not uncommon in the Dutch subsurface. This means that the method of numerical dispersion reduction through increasing grid cell size and time step resolution, might not be practically feasible

for reservoir models of different type and larger size than the one used in this thesis. Furthermore, the mixing behavior of the reservoir modeled in this thesis is case specific, meaning that the results on substitution of physical dispersion with numerical dispersion can not simply be generalized to reservoirs with different sizes and characteristics. For example, the possibility for substitution of the effect of physical dispersion, by numerical dispersion at a cell size of 10 m, is only valid for the reservoir and injection and production characteristics discussed in section 5.3.4. If one wishes to use this method for a reservoir with different dimensions and characteristics, a new sensitivity analysis should be conducted to the effects of physical and numerical dispersion. Furthermore, the possibility of substitution has been investigated for one storage cycle, meaning that it is still unsure if the same substitution gives reasonably similar results after for example ten storage cycles.

The used model in this study has a homogeneous distribution of its reservoir properties, which will not be the case in a more realistic representation of gas reservoirs. The implementation of heterogeneous permeability in the reservoir model might result in different mixing behavior. The dispersivity value in the reservoir simulator can only be varied between longitudinal and transverse directions, and no varying dispersivity value within these directions is possible, which is the case in reality. This leads to a homogenized effect of mechanical dispersion in the model.

The homogeneous model in this thesis is meant to create a conceptual understanding in the physics involved in the process of mixing in UHS operations in gas reservoirs. The thesis is a foundation for further research, in which the challenges of realistically implementing the UHS mixing processes in a reservoir simulator are identified and demonstrated, rather than a detailed analysis of a multi-cycle storage scenario in which exact numbers of the production properties are obtained.

6.2.3. RECOMMENDATIONS

As mentioned in section 6.2.2, this thesis is meant to create a conceptual understanding of the mixing processes taking place in UHS in gas reservoirs, and their implementation in a reservoir simulator. Before any further detailed analysis can be done with more complicated heterogeneous reservoirs including multiple storage cycles, more data should be collected on the behavior of mechanical dispersion at field scale. From the literature that was reviewed on the topic of dispersion, it became clear that none of the authors was completely sure of dispersivity values being applicable at specific reservoir length scales, especially at a scale larger than 300 m. It is not clear above which length scale mixing should be attributed to and modeled with other heterogeneities than those related to dispersivity. There is a need for general consensus on this topic, and further modeling and experimental work should focus on this. It could consist of longtime large scale carefully planned tracer experiments with well defined solute input, accompanied by the related modeling work on realistically representing physical dispersion in simulations.

The effect of permeability and reservoir dimensions on the extent of gravitational segregation during the first storage cycle has been demonstrated. The recommended continuation is to quantify the gravitational segregation by the gravity number described in eq. (2.10.1). By evaluating the development of the gravity number for specific operating schemes, at specific reservoir dimensions, a better estimation could be made about the gas mixing behavior in terms of gravitational segregation.

Furthermore, modelling experiments should be undertaken with the goal of minimizing the effects of numerical dispersion on mixing, while maintaining practical computational times. The recommended direction is to implement and use higher order difference equations to solve the advection dispersion equation. The usefulness was tested for this thesis by using a second order scheme in combination with a TVD flux limiter, the latter of which functions to control numerical oscillations caused by the higher order method. It is recommended to experiment with even higher order schemes to bring down numerical dispersion to levels negligible compared to physical dispersion.

If sufficient reduction of numerical dispersion as described above proves to be unrealistic in the near future, it is recommended to further explore the method of substituting physical dispersion with numerical dispersion. In this thesis it was proven that this substitution can be done for the first storage cycle in a homogeneous radial reservoir. However, further research is needed to prove if the similarity between numerical and physical

dispersion for a specific grid size will hold throughout multiple storage cycles and for heterogeneous reservoirs.

Bibliography

[1] N. P. Brandon and Z. Kurban, Philosophical Transactions of the Royal Society A: Mathematical, Physical and Engineering Sciences **375** (2017), 10.1098/rsta.2016.0400.

[2] S. van Gessel, J. Juez Larré, T. Huijskes, and R. Dalman, "Ondergrondse energieopslag in nederland 2030 – 2050: Ontwikkelpaden en aanbevelingen," (2021), eBN-TNO-rapport.

[3] M. S. Costanza-Robinson and M. L. Brusseau, Water Resources Research **38** (2002), 10.1029/2001wr000895.

[4] L. W. Gelhar, C. Welty, and K. R. Rehfeldt, Water Resources Research **28** (1992), 10.1029/92WR00607.

[5] e. DBI GmbH and N. EZK, "The effects of hydrogen injection in natural gas networks for the Dutch underground storages," (2017).

[6] U. Nations, "Sustainable development goals report 2021," https://unstats.un.org/sdgs/report/2020/ (2021), paris Climate Agreement.

[7] E. Union, "2030 climate energy framework," https://ec.europa.eu/clima/policies/strategies/2030_en (2021), regulation on the Governance of the Energy Union and Climate Action.

[8] J. Gigler, M. Weeda, R. Hoogma, and J. de Boer, "Hydrogen for the energy transition, a programmatic approach for hydrogen innovations in the netherlands," (2019), for the 2020-2030 period.

[9] R. Weijermars and S. M. Luthi, "Dutch natural gas strategy: Historic perspective and challenges ahead," (2011).

[10] D. Zivar, S. Kumar, and J. Foroozesh, International Journal of Hydrogen Energy (2020), 10.1016/j.ijhydene.2020.08.138.

[11] S. van Gessel, J. Breunese, J. Juez Larré, T. Huijskes, and G. Remmelts, "Ondergrondse opslag in nederland," (2018), eBN-TNO-rapport.

[12] B. Hagemann, M. Rasoulzadeh, M. Panfilov, L. Ganzer, and V. Reitenbach, Computational Geosciences **20** (2016), 10.1007/s10596-015-9515-6.

[13] A. Amid, D. Mignard, and M. Wilkinson, International Journal of Hydrogen Energy **41** (2016), 10.1016/j.ijhydene.2016.02.036.

[14] P. A. Dickey, "Petroleum development geology," (1981), united States.

[15] U. Bünger, J. Michalski, F. Crotogino, and O. Kruck, in *Compendium of Hydrogen Energy* (2016).

[16] B. Hagemann, M. Rasoulzadeh, M. Panfilov, L. Ganzer, and V. Reitenbach, Environmental Earth Sciences **73** (2015), 10.1007/s12665-015-4414-7.

[17] W. T. Pfeiffer and S. Bauer, in *Energy Procedia*, Vol. 76 (2015).

[18] F. Feldmann, B. Hagemann, L. Ganzer, and M. Panfilov, Environmental Earth Sciences **75** (2016), 10.1007/s12665-016-5948-z.

[19] A. Sainz-Garcia, E. Abarca, V. Rubi, and F. Grandia, International Journal of Hydrogen Energy **42** (2017), 10.1016/j.ijhydene.2017.05.076.

[20] B. Hagemann, "Numerical and analytical modeling of gas mixing and bio-reactive transport during underground hydrogen storage," (2018), vol.50.Cuvillier Verlag.

[21] B. Srinivasan, "The impact of reservoir properties on mixing of inert cushion and natural gas in storage reservoirs," (2006), graduate Theses, Dissertations, and Problem Reports. 3238.

[22] J. Blicharski and C. Rybicki, Archives of Mining Sciences **53** (2008).

[23] V. K. Shrivastava, L. X. Nghiem, R. G. Moore, and T. Okazawa, "Modelling physical dispersion in miscible displacement - Part 1: Theory and the proposed numerical scheme," (2005).

[24] J. R. Fanchi, Society of Petroleum Engineers journal **23** (1983), 10.2118/9018-PA.

[25] A. P. Hollis, JPT, Journal of Petroleum Technology **36** (1984), 10.2118/12932-PA.

[26] R. C. Reid, T. K. Sherwood, and R. E. Street, Physics Today **12** (1959), 10.1063/1.3060771.

[27] "https://www.e-education.psu.edu/png550/node/840," (2020), pennsilvania college of earth and mineral sciences.

[28] W. L. Hosch, "Brownian motion physics," (1996, Britannica).

[29] D. Schulze-Makuch, "Longitudinal dispersivity data and implications for scaling behavior," (2005).

[30] H. S. Salem and G. V. Chilingarian, Journal of Petroleum Science and Engineering **23** (1999), 10.1016/S0920-4105(99)00009-1.

[31] A. Arya, T. A. Hewett, R. G. Larson, and L. W. Lake, SPE RESERVOIR ENGNG. **3** (1989), 10.2118/14364-pa.

[32] F. Molz, "Advection, dispersion, and confusion," (2015).

[33] H. Hajibeygi, "Tudelft, aesm1325, diffusion/dispersion in porous media," `https://brightspace.tudelft.nl/d2l/le/content/192303/viewContent/1581512/View` (2019), accessed: 2021–02.

[34] UserguideCMG, GEM Software manual , CalgaryCanada (2006-2020).

[35] D. W. Peaceman, "Effective transmissibilities of a gridblock by upscaling - Comparison of direct methods with renormalization," (1997).

[36] M. R. Tek, *Applied sciences Vol. 171* (1989).

[37] V. Vilarrasa, D. Bolster, M. Dentz, S. Olivella, and J. Carrera, Transport in Porous Media **85** (2010), 10.1007/s11242-010-9582-z.

[38] M. Dentz and D. M. Tartakovsky, Transport in Porous Media **79** (2009), 10.1007/s11242-008-9268-y.

[39] D. Y. Peng and D. B. Robinson, Industrial and Engineering Chemistry Fundamentals **15** (1976), 10.1021/i160057a011.

[40] G. S. Shiralkar and R. E. Stephenson, SPE Reservoir Engineering (Society of Petroleum Engineers) **6** (1991), 10.2118/16975-pa.

[41] J. Cordazzo, C. R. Maliska, A. da Silva, C. R. Maliska, and A. Fabio, 2nd Meeting on Reservoir Simulation, Buenos Aires, November 5-6, 2002 (2002).

[42] H. Hoteit, M. Fahs, and M. R. Soltanian, Geosciences (Switzerland) **9** (2019), 10.3390/geosciences9050199.

[43] S. D. R. R. G. G. R. Juez-Larré, J. Gessel, "Assesment of underground energy storage potential to support the energy transition in the netherlands," .

[44] M. P. Pichler, in *Sustainable Earth Sciences, SES 2013: Technologies for Sustainable Use of the Deep Sub-Surface* (2013).

I

APPENDICES

A | Derivations

A.1. 1D Advection/Dispersion derivations

The 1D advection/dispersion equation is derived from the general advection/dispersion equation 2.2.1 as follows.

$$\phi\frac{\partial C}{\partial t}+\nabla Cu-\nabla(D_h\nabla C)\phi=0$$

For which,

$$\nabla Cu=\frac{\partial Cu_x}{\partial x}=\frac{C\partial u_x}{\partial x}+\frac{u_x\partial C}{\partial x}$$

For which $\frac{\partial Cu_x}{\partial x}=0$, due to constant flow speed.

Now, in order to solve $-\nabla(D\nabla C)\phi$, first ∇C must be solved. $\nabla C=\frac{\partial C}{\partial x}$

The dispersion coefficient D_h for a 1D system is constant because of the assumed homogeneity on reservoir scale. Nevertheless, on pore scale there exists heterogeneity, which is the cause for dispersion.

The dimensionless advection/dispersion equation is as follows:

$$0=\frac{\partial C_D}{\partial t_D}+\frac{\partial C_D}{\partial x_D}-\frac{1}{\frac{U_xL}{\phi D_h}}\left(\frac{\partial^2 C_D}{\partial x_D^2}\right)$$

where the dimensionless parameters are defined as below:

$$t_D=\frac{u_xt}{\phi L}=\frac{qt}{A\phi L}$$

$$X_D=\frac{x}{L}$$

$$C_D=\frac{C(x,t)-C(i)}{C(j)-C(i)}$$

A.2. 2D Advection/Dispersion derivations

In order to compare a 2D-radial system to the earlier analyzed 1D system for hydrogen gas injection, the divergences in eq. (2.2.1) must be simplified. The term $\phi\frac{\partial C}{\partial t}$ is already in the desired form.

$$\nabla Cu=\frac{1}{r}\frac{\partial(rCu_r}{\partial r}+\frac{1}{r}\frac{\partial Cu_\theta}{\partial\theta}+\frac{\partial Cu_z}{\partial z}$$

We are assuming a 2D radial system, which is homogeneous on reservoir scale, where the flow velocity is decreasing as the injected gas propagates outward. However, the flow velocity and concentration are assumed equal on all angles θ and there is no z-component as we are observing a 2D system. Therefore, ($\frac{\partial Cu_\theta}{\partial\theta}=0$ and $\frac{\partial Cu_z}{\partial z}=0$

$$\nabla Cu=\frac{1}{r}\frac{\partial(rCu_r}{\partial r}=\frac{1}{r}\left(\frac{(rC\partial u_r)}{\partial r}+\frac{Cu_r\partial r}{\partial r}+\frac{ru_r\partial C}{\partial r}\right)$$

Due to $\frac{\partial r}{\partial r}=1$, $\frac{1}{r}\left(\frac{(rC\partial u_r)}{\partial r}+\frac{Cu_r\partial r}{\partial r}+\frac{ru_r\partial C}{\partial r}\right)$ simplifies to $\frac{C\partial u_r}{\partial r}+\frac{u_r\partial C}{\partial r}+\frac{Cu_r}{r}$

Now, in order to simplify $-\nabla(D_h\nabla C)\phi$, first ∇C must be simplified:

$$\nabla C = \frac{1}{r}\frac{\partial(rC)}{\partial r} = \frac{1}{r}\left(\frac{C\partial r}{\partial r} + \frac{r\partial C}{\partial r}\right)$$

Due to $\frac{\partial r}{\partial r} = 1$, $\frac{1}{r}\left(\frac{C\partial r}{\partial r} + \frac{r\partial C}{\partial r}\right)$ simplifies to: $\left(\frac{C}{r} + \frac{\partial C}{\partial r}\right)$

$$-\phi\nabla(D_h\nabla C) = -\phi\frac{1}{r}\frac{\partial(rD_h\nabla C}{\partial r} = -\phi\frac{1}{r}\left(\frac{rD_h\partial(\nabla C)}{\partial r} + \frac{r\nabla C\partial(D_h)}{\partial r} + \frac{D_h\nabla C\partial(r)}{\partial r}\right) = -\phi\frac{D_h\partial(\nabla C)}{\partial r} - \phi\frac{\nabla C\partial(D_h)}{\partial r} - \phi\frac{D_h\nabla C}{r}$$

After substituting $\left(\frac{C}{r} + \frac{\partial C}{\partial r}\right)$, which was simplified from ∇c, $-\phi\nabla(D_h\nabla C)$ this becomes:

$$= -\phi\frac{D_h\partial(\frac{c}{r} + \frac{\partial C}{\partial r})}{\partial r} - \phi\frac{(\frac{C}{r} + \frac{\partial C}{\partial r})\partial(D_h)}{\partial r} - \phi\frac{D_h(\frac{C}{r} + \frac{\partial C}{\partial r}}{r}$$

$$= -\phi\frac{D_h\partial C}{\partial r} - \phi\frac{D_h\partial^2 C}{\partial r^2} - \phi\frac{C}{r}\frac{\partial D_h}{\partial r} - \phi\frac{\partial C}{\partial r}\frac{\partial D_h}{\partial r} - \phi\frac{D_h C}{r^2} - \phi\frac{D_h}{r}\frac{\partial C}{\partial r}$$

Therefore, the total 2D advection-dispersion equation becomes eq. (2.6.1):

$$\phi\frac{\partial C}{\partial t} + \frac{C\partial u_r}{\partial r} + \frac{u_r\partial C}{\partial r} + \frac{Cu_r}{r} - \phi\frac{D_h\partial C}{\partial r} - \frac{D_h\partial^2 C}{\partial r^2} - \phi\frac{C}{r}\frac{\partial D_h}{\partial r} - \phi\frac{\partial C}{\partial r}\frac{\partial D_h}{\partial r} - \phi\frac{D_h C}{r^2} - \phi\frac{D_h}{r}\frac{\partial C}{\partial r} = 0$$

$$\phi\frac{\partial C}{\partial t} + \left(u_r - \frac{\phi D_h}{r} - \phi D_h - \frac{\phi\partial D_h}{\partial r}\right)\frac{\partial C}{\partial r} + \frac{C\partial u_r}{\partial r} - \phi\frac{D_h\partial^2 C}{\partial r^2} - \phi\frac{\partial C}{r}\frac{\partial D_h}{\partial r} + \frac{rCu_r - \phi D_h C}{r^2} = 0$$

B | Additional results

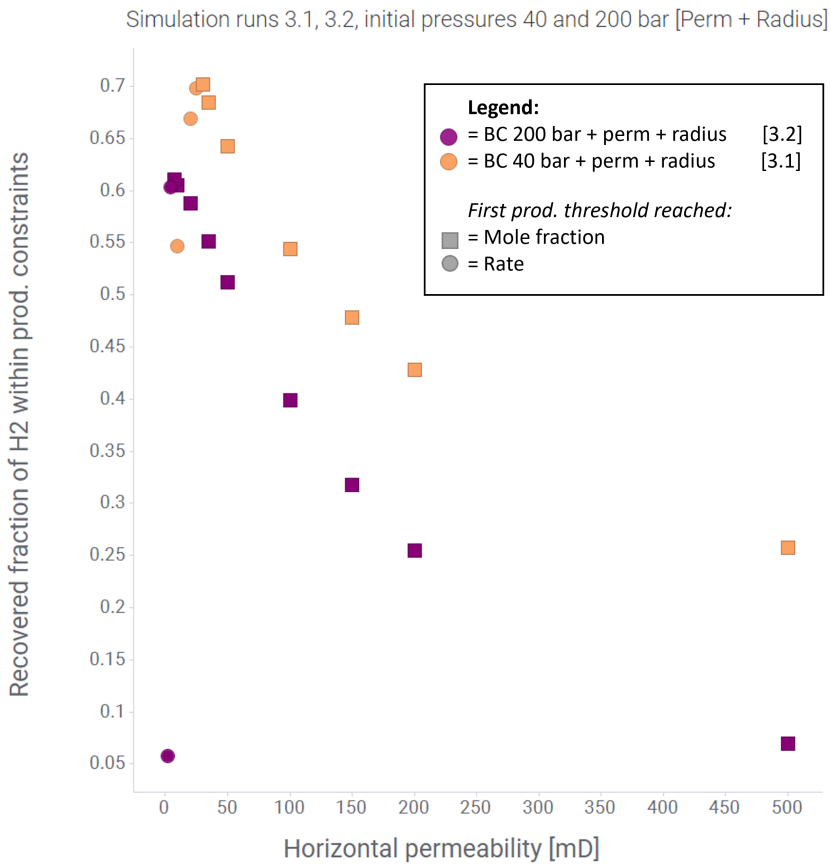

Figure B.1: Results from the chapter 4 simulations. This plot shows the results for doubling the reservoir radius.

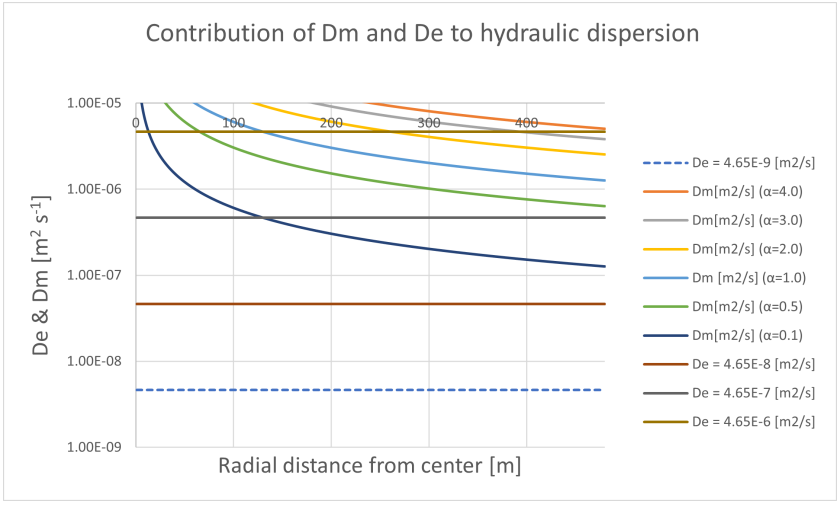

Figure B.2: Contributions of D_m and D_m to D for dispersivity range [0.1-0.4] and effective molecular diffusion from $4.65E-9 m^2 s^{-1}$ up to $4.65E-6 m^2 s^{-1}$

C | Figures and diagrams

Year	Title	Authors	Subject	Main goal	Main Findings
2016	Seasonal storage of hydrogen in a depleted natural gas reservoir	A.Amid, D.Mignard, M.Wilkinson	Production characteristics	Preliminary assesment of feasibility of storing hydrogen in gas reservoirs after natural gas production ceases. Emphasis on WGC and prod. Rate	WGC/TGC and flow rate could be higher for hydrogen than natural gas. But higher energy content of natural gas makes average energy output of hydrogen 40% of natural gas for 120 days storage
2013	Assesment of Hydrogen Rock Interaction During Geological Storage of CH4-H2 Mixtures	M.P. Pichler	Biochemical	Asses the interaction of H2 with storage formation	
2020	Seasonal hydrogen storage in depleted gas reservoirs	T. Visser	Mixing behavior	Identification and adressing of potential losses during H2 storage. Analysing hydrodynamic behaviour of H2 in contact with other gasses through gravity number. And cyclic storage	Bacterial conversion biggest challenge for long term storage. Displacement of H2 towards residual gasses is most efficient when dominated by viscous forces. A higher difference between injection and production pressure leads to lower cyclic efficiency.
2020	EAGE GET presentation Walter + Thijs	W.Eikelenboom, T. Huijskes	Production characteristics	Learn how hydrogen properties change the performance of the reservoir in terms of WV:CV and flow rate above certain thresholds.	higher kh means higher WV:CV up to certain value. WV:CV ratio changes in specific ways when reservoir dimension is varied and high perm streaks etc.
2016	Large scale underground hydrogen storage for the grid integration of renewable energy and other applications	U. Bünger, J. Michalski	long term context	Overview of all possible underground starage solutions.	Small piece on hydrogen in porous media underground structures. Mainly discusses the expected development of certain types of fields at specific moments in the future for hydrogen storage
2015	Mathematical modeling of unstable transport in underground hydrogen storage	B.Hageman, M.Panfilov	Mixing behavior	Demonstrating that besides microbial activities, the hydrodynamic behaviour of UHS is different from UGS.	For high injection rates, viscous forces are dominant and hydrogen will spread laterally beyond cap rock and be lost. Lower injection rates have dominating gravitational forces. WATER SATURATED RESERVOIR
2016	Numerical simulation of hydrodynamic and gas mixing processes in underground hydrogen storages	F.Feldmann, B.Hagemann	Mixing behavior	mixing effects between hydrogen and other gases in the reservoir. Nitrogen is introduced as cushion gas.	Together with diffusion, dispersion leads to amplified mixing of gas components. Gravity overide and fiscous fingering play much less of a role in empty gas reservoir than in aquifers
2015	Subsurface porous media hydrogen storage – scenario developmentand simulation	W.T.Pfeiffer, S. Bauer	Mixing behavior + Production characteristics	Investigate the system behaviour of a hypothetical subsurface porous media hydrogenstorage site in northern Germany using numerical scenario simulations	Storage performance increases from first to fourth cycle and is able to contribute a large portion of the electricty demand in german province.
2015	Hydrogenization of underground storage of natural gas	B.Hageman, M.Panfilov	Biochemical + mixing behavior	Show that there are large differences between UGS and UHS which arise due to the particular hydrodynamic and bio-chemical characteristics.	Hydrogen is a universal electron donor for the metabolism of different microbial species, which are present in subsurface structures. Hence, the injection of hydrogen stimulates their activity and problems could arise. Hydrodynamic behaviour is dominated by viscous or gravitational forces, depending on the injection rate. (multy-phase)
2018	Ondergrondse Opslag in Nederland – Technische Verkenning	T.Huijskes	Feasibility study	Quantitative description of the demand and supply for underground storage in the netherlands.	Estimated storage supply in empty gas fields of 93 billion m3 in onshore fields. 60 billion m3 offshore fields. Demand estimated 10 billion m3 total H2 storage

Figure C.1: Literature research table

Year	Title	Authors	Subject	Main goal	Main Findings
2017	The effects of hydrogen injection in natural gas networks for the Dutch underground storages	Netherlands Enterprise Agency	Feasibility study	Similar to Nr. 10 but also some field specific parameters on PGI and other Dutch UGS fields	A lot of information on Dutch gas fields that are used for gas storage
2008	The gas mixing process in underground gas storages	J.Blicharski	Mixing behavior	Correlating results of nitrogen concentrations in withdrawn gas for initial five operating cycles at UGS Wierzchowice Poland	Determining molecular diffusion coefficients and the dispersivities for individual wells. Determining the position of the displacement front
1983	A Laplace transform technique for the analytical solution of a diffusion- convection equation over a finite domain	G.B. Davis	Mathematics	Presenting two correct versions of analytic solutions of a diffusion-convection equation over a finite domain.	Full analytical solution
2020	Underground hydrogen storage: a comprehensive review	D. Zivar, S. Kumar	Feasibility study	Reviews technical aspects and feasibility of UHS. Very broad, not technically deep.	Preliminary assesment at basin scale needed to find suitable site for starage bases on the capacity, reseroir and fluid properties and other site screening criteria.
2004	Hydrogen storage methods	A. Züttel	Storage options	Deep technical evaluation of non-subsurface storage of Hydrogen	Best materials can handle 150 kg/m3. Could be improved by 50% by now. According to estimations
2017	Numerical and analytical modeling of gas mixing and bio-reactive transport during underground hydrogen storage	B. Hagemann	Biochemical + mixing behavior	Quantitative evaluation of biochemical and mixing behavior of hydrogen in subsurface storage	Tendency to gravity override and viscous fingering in aquivers. During gas displacement, strong mixing between by molecular diffusion and mechanical dispersion.
1963	A review of Diffusion and Dispersion in porous media	T.K. Perkins	Physics review	Summarize and interpret information on diffusion and dispersion from literature	Flow through porous media adds to total dispersion. Longitudinal and transversal dispersion equations given.
2006	The impact of reservoir properties on mixing of inert cushion and natural gas in storage reservoirs	B.S. Srinivasan	Mixing behavior	See Title	Mixing mostly influenced by injection rate
2014	An overview of hydrogen underground storage technology and prospects in China	M. Bai	Feasibility study	Feasability study/ summary	Cushion gas ratio's
2017	Assesment of feasibility strategies for seasonal underground hydrogen storage in a saline aquifer	A. Sainz-Garcia	Mixing behavior + Production characteristics	Feasability study with simulation	Maximum hydrogen recovery ratio of 78% in aquifers estimated. Gravity upconing major effect when no other cushion gas used. Shallow extraction wells and steeply dipping structures are key to efficient hydrogen storage
1985	Mixing in Underground Storage Reservoirs	J.F. Carriere	Mixing behavior	Modelling methods and computations for mixing in Storage	The field of mathematical modeling for miscible gas flows still represents a considerable challenge in the area of numerical dispersion
2003	Physical dispersion in compositional reservoir simulation	V.K. Shrivastava	Mixing behavior	Testing a new rigorous dispersive flux-continuous scheme based on a multi-point control volume method, which allows inclusion of the full tensor of physical dispersion	Proving the differences in physical and numerical dispersion, in a theoretical simulation. (non-related to hydrogen storage)
2015	Advection, Dispersion, and Confusion	F. Molz	Mixing behavior	Reviewing the scale dependency of field scale dispersion	The use of scaled up numbers as mentioned in Gelhar et al. 1992 would magnify irreversible mixing way beyond what is seen in the field.
1992	A critical review of data on field-scale dispersion in aquifers	L. W. Gelhar C. Welty, K. R. Rehfeldt	Mixing behavior	Reviewing experimental dispersivity data from previous reports	Experiments are assigned a reliablity and dispersivity is concluded to be experiment scale dependent
2005	Longitudinal Dispersivity Data and Implications for Scaling Behavior	D. Schulze-Makuch	Mixing behavior	Reviewing experimental dispersivity data from previous reports	Scaling exponent and an empirical power low are constructed in order to describe the scale dependency of experimental dispersivity data

Figure C.2: Literature research table extended

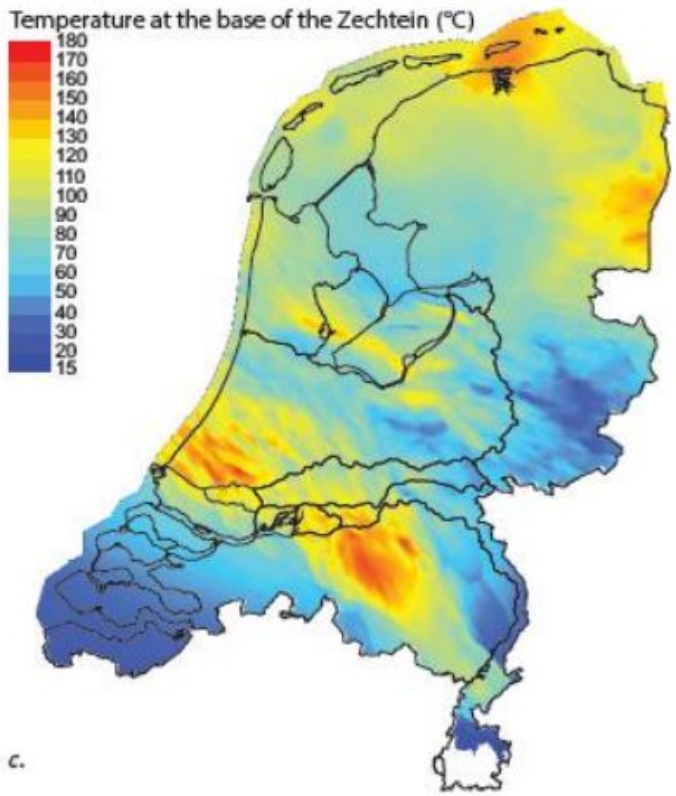

Figure C.3: Temperature at the base of Zechstein C° [5].